AD-A063 990 OHIO STATE UNIV COLUMBUS DEPT OF GEODETIC SCIENCE F/G 22/3
IMPROVED PROCEDURES FOR THE RECOVERY OF 5 DEGREES MEAN GRAVITY --ETC(U)
SEP 78 D P HAJELA F19628-76-C-0010
UNCLASSIFIED DGS-276 AFGL-TR-78-0260 NL

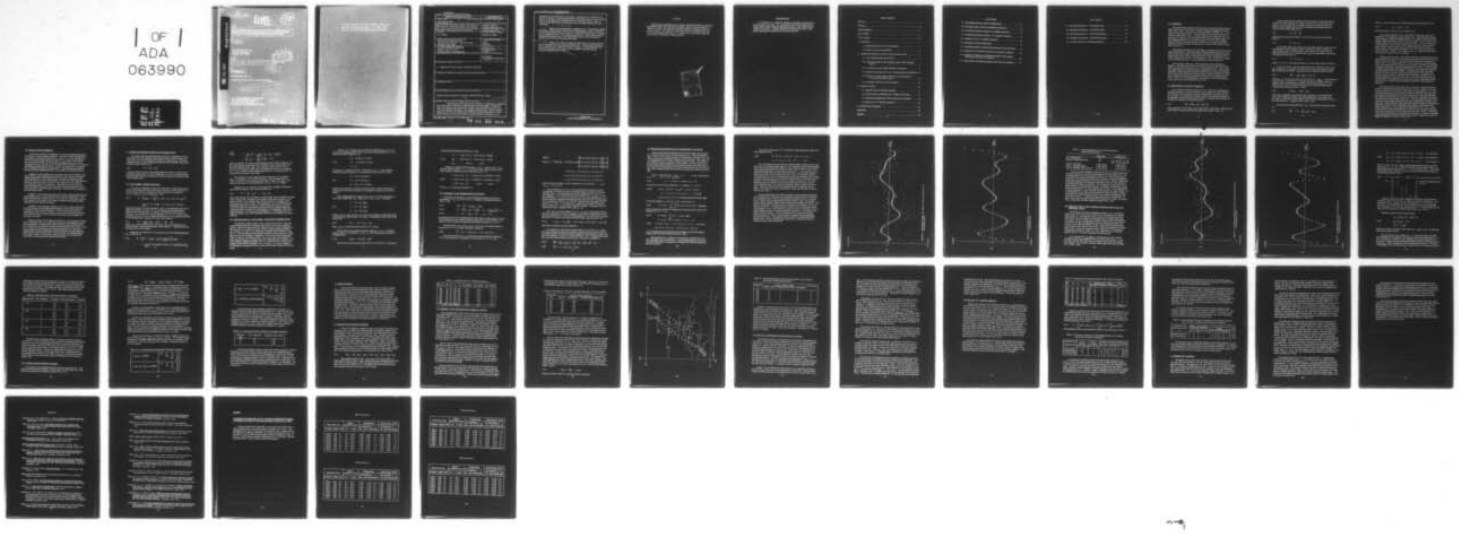

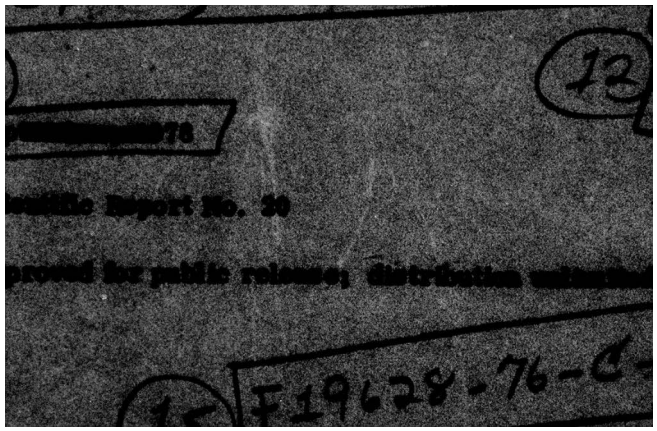
12
F19628-76-C

Unclassified

SECURITY CLASSIFICATION OF THIS PAGE (When Data Entered)

REPORT DOCUMENTATION PAGE		READ INSTRUCTIONS BEFORE COMPLETING FORM
1. REPORT NUMBER AFGL-TR-78-0260	2. GOVT ACCESSION NO.	3. RECIPIENT'S CATALOG NUMBER
4. TITLE (and Subtitle) IMPROVED PROCEDURES FOR THE RECOVERY OF 5° MEAN GRAVITY ANOMALIES FROM ATS-6/GEOS-3 SATELLITE TO SATELLITE RANGE-RATE OBSERVATION USING LEAST SQUARES COLLOCATION		5. TYPE OF REPORT & PERIOD COVERED Scientific. Interim Scientific Report No. 20
		6. PERFORMING ORG. REPORT NUMBER Geodetic Science 276
7. AUTHOR(s) D.P. Hajela		8. CONTRACT OR GRANT NUMBER(s) F19628-76-C-0010
9. PERFORMING ORGANIZATION NAME AND ADDRESS Department of Geodetic Science The Ohio State University - 1958 Neil Avenue Columbus, Ohio 43210		10. PROGRAM ELEMENT, PROJECT, TASK AREA & WORK UNIT NUMBERS 62101F 760003AG
11. CONTROLLING OFFICE NAME AND ADDRESS Air Force Geophysics Laboratory Hanscom AFB, MA 01731 Contract Monitor: Bela Szabo/LW		12. REPORT DATE September, 1978 13. NUMBER OF PAGES 44 pages
14. MONITORING AGENCY NAME & ADDRESS(if different from Controlling Office)		15. SECURITY CLASS. (of this report) Unclassified 15a. DECLASSIFICATION/DOWNGRADING SCHEDULE

16. DISTRIBUTION STATEMENT (of this Report)

A - Approved for public release; distribution unlimited

17. DISTRIBUTION STATEMENT (of the abstract entered in Block 20, if different from Report)

18. SUPPLEMENTARY NOTES

19. KEY WORDS (Continue on reverse side if necessary and identify by block number)

geodesy, gravity anomalies, satellite to satellite tracking, GEOS-3

dot

R - double dot

20. ABSTRACT (Continue on reverse side if necessary and identify by block number)

The prediction of 5° mean gravity anomalies is considered by collocation from ATS-6/GEOS-3 satellite to satellite range-rate observations. The auto and cross-covariances of the residual line of sight accelerations $\ddot{R}$ from GEOS-3 to ATS-6 are computed rigorously in the anomalous potential field. The raw residual range-rate $\dot{R}$ values are filtered and smoothed by approximating them in a least squares sense by a cubic spline function, and the residual accelerations $\ddot{R}$ are

DD FORM 1 JAN 73 1473 EDITION OF 1 NOV 65 IS OBSOLETE

R-dot

Unclassified

obtained as the first derivatives of the spline. Experiments are described to fit the raw $\dot{R}$ values by a spline function with variable knots, and to remove any linear trend from $\ddot{R}$ values due to residual errors in initial state vectors. The correlation coefficients between the predicted values of neighboring anomalies are considered.

Numerical considerations are discussed, and a computational strategy is outlined. Destruct-doppler data with 10 seconds integration time is used from four revolutions between April 26 to May 12, 1975 for predicting eight 5° anomalies in the Caribbean Sea area. The predicted anomalies are compared with anomalies obtained from altimeter data, with terrestrial anomalies, and with anomalies implied by (30, 28) PGS 110 gravitational model.

Inspite of low density of range-rate data directly over the anomalies, and the high noise level of the destruct-doppler data, it appears that 5° anomalies can be predicted with a standard deviation of 6 mgals. It is found that these predicted anomalies agree much better with the altimeter anomalies than the anomalies implied by PGS 110 field.

Foreword

This report was prepared by D.P. Hajela, Research Associate, Department of Geodetic Science, The Ohio State University, under Air Force Contract No. F19628-76-C-0010, The Ohio State University Research Foundation Project No. 4214 B1 (710335). The contract covering this research is administered by the Air Force Geophysics Laboratory, L.G. Hanscom Air Force Base, Massachusetts, with Mr. Bela Szabo, Contract Monitor.

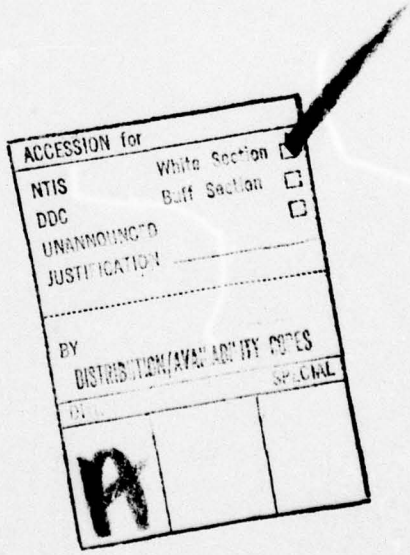

Acknowledgement

I am indebted to Dr. Richard H. Rapp for his guidance and comments at various stages of this study. Mr. James Marsh of the NASA Goddard Space Flight Center supplied important information relative to the orbital elements of GEOS-3 and ATS-6. I greatly appreciate the discussions with Dr. Hans Sünkel regarding the computation of covariance functions.

Table of Contents

List of Tables

List of Figures

1. Introduction

We consider the recovery of 5° mean gravity anomalies from the doppler signal count in the ATS-6/GEOS-3 satellite to satellite tracking (SST) (NASA, 1974; Kaula, 1969). The doppler count was obtained at Rosman, N.C. in the 'destruct' mode (NASA, 1976). The actual data will be described in Section 3. Eddy and Sutermeister (1975, p. 43) have shown that the range-rate sum, $\dot{R}_s$ (Martin, 1972; Hajela, 1974) is directly obtained from the doppler count. We accordingly consider $\dot{R}_s$ to be the observations, which were used to predict gravity anomalies using least squares collocation, according to procedures developed in Rummel, Hajela and Rapp (1976). These will be briefly recapitulated in Section 1.1.

The present study follows the investigations by Hajela (1977) and considers improved procedures. The main change is the computation of the auto-covariances of the ATS-6/GEOS-3 'line-of-sight' residual accelerations in the anomalous potential field, and the computation of the cross-covariances of the residual accelerations with the 5° mean anomalies. This, and the other changes will be outlined in Section 1.2, and developed more fully in Section 2.

The numerical evaluation of these procedures will be described in Section 3. The numerical evaluation is based on the initial state vectors for ATS-6 and GEOS-3 for some of the 'arcs' used by Marsh et als. (1977), which were kindly supplied by Marsh (private communication, 1978). The predicted anomalies will be compared with those obtained from the altimeter data (Rapp, 1977), from the terrestrial observations (Rapp, private communication, 1978), and also against the anomalies implied by the PGS-110 gravity field (Lerch, 1976). The last was the gravitational model employed in the 'determination' of the initial state vectors (Marsh et als., 1977).

1.1 Recapitulation of Previous Investigations

The procedure developed by Rummel et als. (1976) was to integrate the equations of motion of ATS-6 and GEOS-3 in a low degree and order reference gravitational field (specifically, potential coefficients up to degree and order 12 were used). This provided the inertial position and velocity coordinates of the satellites at any given time, and from which a computed value of range-rate sum $\dot{R}_s^c$ was obtained in the reference field, U.

$$\dot{R}_s^c = \tfrac{1}{2}(\dot{R}_{1u} + \dot{R}_{2d} + \dot{R}_{2u} + \dot{R}_{1d}) \tag{1.1}$$

where subscripts 1 and 2 refer to ATS-6 and GEOS-3 respectively, and subscripts u and d refer to upward and downward range-rates (Hajela, 1974, p. 8).

It was assumed that the reference field was adequate to fully describe the motion of the ATS-6 satellite at a height of about 35,000 km above the earth's surface. If we then subtract $\dot{R}_s$ computed in the reference field U from the observed value of range-rate sum, $\dot{R}_s^o$, in the actual gravitational field of the earth, W, the residual range-rate $\dot{R}$

$$\dot{R} = \dot{R}_s^o - \dot{R}_s^c \tag{1.2}$$

describes the range-rate of GEOS-3 to ATS-6 in the anomalous gravitational field, T:

$$T = W - U \tag{1.3}$$

The residual range-rate $\dot{R}$ was numerically differentiated to obtain residual accelerations $\ddot{R}$ in the anomalous field T. Knowing the angle α between the 'line of sight' GEOS-3 to ATS-6 and the radial direction at GEOS-3 from the satellites ephemeris in the reference field, we have the approximate relationship (for details, see Section 2.1):

$$T_r \doteq \ddot{R} / \cos \alpha \tag{1.4}$$

where $T_r \equiv \partial T / \partial r$ is the first derivative of T in the radial direction at GEOS-3.

A set of $\underline{T}_r$ values, when the sub-satellite point of GEOS-3 is in the immediate vicinity of a 5° anomaly, were then used to predict the residual anomaly, $\hat{\Delta g}'$, in the reference field U, using least squares collocation (Moritz, 1972):

$$\hat{\Delta g}' = \underline{C}^T_{\Delta g, T_r} \, (\underline{\underline{C}}_{T_r, T_r} + \underline{\underline{D}})^{-1} \, \underline{T}_r \tag{1.5}$$

where $\underline{\underline{C}}_{T_r, T_r}$ is the auto-covariance matrix of vector $\underline{T}_r$, $\underline{C}^T_{\Delta g, T_r}$ is the transposed vector of cross-covariances of $\underline{T}_r$ with the mean gravity anomaly, and $\underline{\underline{D}}$ is a diagonal matrix representing the variance of observational noise in $\underline{T}_r$. The predicted value $\hat{\Delta g}'$ of the residual anomaly in the reference field could be compared with its expected value, $E(\Delta g')$:

$$E(\Delta g') = \Delta g_\varepsilon - \Delta g_U \tag{1.6}$$

where Δg_ε represents the gravity anomaly referred to an ellipsoidal field, e.g. Geodetic Reference System 1967, and available from, say, Rapp (1977); and Δg_U is the gravity anomaly implied by the potential coefficients (12, 12) of the reference field U. (Rummel et als., 1976, p. 20).

The estimated standard deviation, $\hat{\sigma}_{\Delta g'}$, of the predicted anomaly is given by:

$$\hat{\sigma}^2_{\Delta g'} = C_0 - \underline{C}^T_{\Delta g, T_r} \, \underline{\underline{C}}^{*-1} \, \underline{C}_{\Delta g, T_r} \tag{1.7}$$

where C_o is the variance of the residual anomalies of that block size, and

$$\underline{\underline{C}}^* = \underline{\underline{C}}_{T_r, T_r} + \underline{\underline{D}} \tag{1.8}$$

and other notation is the same as in equation (1.5).

It was found in Rummel et als. (1976) that the matrix $\underline{\underline{C}}^*$ could not be inverted for zero standard deviation of noise in $\underline{T}_r$. The inversion was numerically stable for standard deviation between 0.5 to 1 mgals, but the predicted anomaly $\hat{\Delta g}'$ was damped, with low root mean square (R.M.S.) value, as the standard deviation was increased to 2 mgals or larger. It was also found that it was adequate to use $\underline{T}_r$ values within a spherical distance of $3^\circ.5$ from the center of the 5° anomaly block, and very little improvement was found if further values within a spherical distance of 5° or $7^\circ.5$ from the center of the block were used. Finally, it was adequate to use $\underline{T}_r$ values at a time interval of 30 seconds, instead of every 10 seconds.

These procedures (ibid., 1976) were developed for simulated data with no observational noise in $\dot{R}$, and further with no assumed errors in the initial state vectors of the two satellites. The effect of these errors was investigated by Hajela (1977). The observational noise in $\dot{R}$ was filtered out by approximating it by a cubic spline in the least squares sense, giving a smoothed representation of $\dot{R}$ which could then be analytically differentiated to give $\ddot{R}$. It was found that a suitable representation was obtained if the knots of the spline were specified at a fixed interval of 60 to 80 seconds. A shorter spacing gave oscillating values of $\ddot{R}$, while a longer spacing gave damped values. The knots of the spline are defined where two adjacent cubic polynomials, and their first and second derivatives, assume the same value. It was also found that $\ddot{R}$ values at either ends of the spline had spuriously large values, and the spline should thus be fitted to a larger data span than what is needed for the prediction of anomalies.

The 'determination' of the initial state vectors was a critical procedure. These are determined through an iterative process for a minimum variance of misfit of observed value (of range, range-rate, or range-rate sum, etc.) after rejecting outlying observations, from the modelled value based on a specified force model and the initial state vectors in the previous step of the interation. The iteration is continued till successive corrections to the initial state vectors lie within a specified tolerance (usually 2%). The converged value of the initial state vectors is strongly influenced by the type of observations, and their total time span. Range-rate sum observations were the least sensitive to determining initial state vectors of the two satellites, and a short time span such as 60 minutes may lead to a very wrong state vector (Hajela, 1977, p. 16). Even if several different types of observations are used, a short time span of observations may seriously bias the determination of initial state vectors. Unavoidably small errors of 10-20 meters in position and 1-2 cm/sec. in velocity coordinates in the determination of the initial state vectors lead to a linear error in the residual accelerations $\ddot{R}$ (ibid., 1977, p. 64).

1.2 Scope of Current Investigations

In the above mentioned investigations, we had only considered the radial derivative T_r of the anomalous potential T. This led to simple computation of the required covariances (Rummel et als., 1976, p. 12), but it had an unduly restrictive implicit assumption that at GEOS-3, at a height of about 850 km above the earth's surface, the derivatives of T perpendicular to the radial direction were zero. We will now also consider these derivatives of T along the latitudinal and longitudinal directions, T_φ and T_λ respectively in computing the covariances of residual accelerations $\ddot{R}$. This follows the treatment by Rummel and Rapp (unpublished notes, 1977) and will be detailed in Section 2.

Secondly, we will consider if we can extract from the raw $\dot{R}$ data 'better' values of $\ddot{R}$, by approximating the raw $\dot{R}$ data by a cubic spline with variable spacing of the knots. With a fixed spacing of the knots, the spline fits the entire data span in the least squares sense. We may start with a fixed spacing, and then let one knot vary at a time for a least squares fit in two adjacent cubic polynomial intervals of the spline. The entire data span can then be 'swept' successively from one end to the other achieving a minimum variance fit in each portion of the data span successively. This follows the treatment of deBoor and Rice (1968).

Thirdly, we will consider the removal of a linear trend from $\ddot{R}$ values due to unavoidable errors in the initial state vectors of ATS-6 and GEOS-3. This follows the treatment of Moritz (1972, p. 78), where the 'observations' may be first 'centered' by the removal of the effect of systematic parameters before using them in least squares collocation.

Fourthly, we will attempt to examine if a set of $\underline{T}_r$ values, which could be used to predict several neighboring anomalies, would cause unduly large correlations in the predicted anomalies. This question may be raised in deciding if a certain anomaly block size may not be recovered from given data, say at GEOS-3 location, if the correlation coefficients between neighboring anomalies are 'large'.

These four points will be discussed in Section 2. Some numerical results will be presented in Section 3, where additional numerical considerations will also be mentioned. The first three points were numerically evaluated in the force model and with initial state vectors as used in Marsh et als. (1977). However, as there was some delay in the receipt of this data, the fourth point regarding the correlation between the predicted anomalies was examined with respect to data used in Hajela (1977), which was based on a slightly different force model. However, as the latter was also based on real $\dot{R}_s$ data, the conclusions are equally valid for improved force fields.

2. Residual Accelerations of GEOS-3 in the Anomalous Field

We consider that the inertial position and velocity coordinates of ATS-6 and GEOS-3 have been obtained in the reference field (complete to degree and order 12) at times corresponding to the observed range-rate sum $\dot{R}_s^o$, and a computed value $\dot{R}_s^c$ in the reference field has also been obtained at these times. Then the residual range-rate $\dot{R}$

$$\dot{R} = \dot{R}_s^o - \dot{R}_s^c \tag{2.1}$$

is the time derivative of the line-of-sight range from GEOS-3 to ATS-6 in the anomalous potential field T in view of equations (1.1) to (1.3), considering that the position and velocity coordinates for the ATS-6 satellite are fully described in the reference field.

2.1 'Line-of-Sight' Residual Acceleration

We would now explicitly consider the residual line of sight acceleration of GEOS-3 in the anomalous field T as the time derivative of $\dot{R}$ in equation (2.1). Let the inertial position coordinates of ATS-6 and GEOS-3 be denoted by X_1, Y_1, Z_1 and X_2, Y_2, Z_2 respectively. Then

$$\dot{R} = \frac{d}{dt}|\underline{R}_{21}| = \frac{d}{dt}\left[(X_1 - X_2)^2 + (Y_1 - Y_2)^2 + (Z_1 - Z_2)^2\right]^{\frac{1}{2}} \tag{2.2}$$

$$= \frac{1}{|\underline{R}_{21}|}\left[-(X_1 - X_2)\dot{X}_2 - (Y_1 - Y_2)\dot{Y}_2 - (Z_1 - Z_2)\dot{Z}_2\right]$$

where we note that $\dot{R}$ is a scalar quantity, $|\underline{R}_{21}|$ is the magnitude of the line of sight vector GEOS-3 to ATS-6, $\dot{X}_2, \dot{Y}_2, \dot{Z}_2$ are the velocity components of GEOS-3 in the anomalous field T (and not in the reference field in view of equation (2.1)), and that the velocity components $\dot{X}_1, \dot{Y}_1, \dot{Z}_1$ of ATS-6 in the anomalous field are zero as we consider the motion of ATS-6 to be fully described by the reference field. Equation (2.2) may be rewritten as:

$$\dot{R} = -\frac{1}{|\underline{R}_{21}|}\left[\underline{R}_{21} \cdot \dot{\underline{R}}_2\right] = -\dot{\underline{R}}_2 \cdot \underline{e}_{21} \tag{2.3}$$

where $\underline{e}_{21}$ is the unit vector GEOS-3 to ATS-6, $\dot{\underline{R}}_2$ is the residual velocity vector of GEOS-3 in the anomalous field, and the notation $\cdot$ between the vectors represents their scalar product.

Taking the time derivative of $\dot{R}$ in equation (2.2) and considering equation (2.3), we get $\ddot{R}$ as:

$$\ddot{R} = \frac{d}{dt}\dot{R} = \left[-\underline{R}_{21} \cdot \dot{\underline{R}}_2\right]\left(-\frac{1}{(|\underline{R}_{21}|)^2}\right)\frac{d}{dt}|\underline{R}_{21}| \tag{2.4}$$

$$+ \frac{1}{|\underline{R}_{21}|}\left[-(X_1 - X_2)\ddot{X}_2 - (Y_1 - Y_2)\ddot{Y}_2 - (Z_1 - Z_2)\ddot{Z}_2 + \dot{X}_2^2 + \dot{Y}_2^2 + \dot{Z}_2^2\right]$$

(2.4)
(cont.)
$$= -\frac{1}{|\underline{R}_{a1}|}\dot{R}^2 + \frac{1}{|\underline{R}_{a1}|}\left[-\underline{R}_{a1}\cdot\ddot{\underline{R}}_a + |\dot{\underline{R}}_a|^2\right]$$
$$= -\ddot{\underline{R}}_a\cdot\underline{e}_{a1} + \frac{1}{|\underline{R}_{a1}|}\left[|\dot{\underline{R}}_a|^2 - \dot{R}^2\right]$$

where we note that $\ddot{R}$ is also a scalar quantity like the residual range-rate $\dot{R}$, $\ddot{\underline{R}}_a$ is the residual acceleration vector of GEOS-3 in the anomalous field (and not in the reference field), $|\dot{\underline{R}}_a|$ is the magnitude of the velocity vector of GEOS-3 in the anomalous field, and we note again that the velocity components $\dot{X}_1$, $\dot{Y}_1$, $\dot{Z}_1$ of ATS-6 in the anomalous field are zero. This equation has also been derived by Rummel et als. (1978).

The second term on the right hand side of equation (2.4) is negligibly small. Considering $|R_{a1}|$ as about 35,000 km, residual range-rate $\dot{R}$ as about 0.1 cm/sec, and an arbitrarily large value of $|\dot{\underline{R}}_a|$ as 2 cm/sec, this term is of the order of $[1/35{,}000\times10^5][4-.01]\times10^3 \approx 1\times10^{-6}$ mgals.

Equation (2.4) may therefore be rewritten with a negligibly small approximation for the 'high-low' case of ATS-6/GEOS-3 as:

(2.5)
$$\ddot{R} = -\ddot{\underline{R}}_a\cdot\underline{e}_{a1} = -\underline{\nabla T}\cdot\underline{e}_{a1}$$

which shows that the time derivative of residual range-rate may indeed by termed as the 'line of sight' component of the residual acceleration of GEOS-3 in the anomalous field. If we consider that at GEOS-3 location at a height of about 850 km above the earth's surface, the components of $\underline{\nabla T}$ in the latitudinal and longitudinal directions are zero (or, in other words, the deviation of vertical is zero with respect to the reference field described by potential coefficients complete to degree and order 12), then equation (2.5) degenerates to the approximate equation (1.4) used in previous investigations. We would however now explicitly consider $\underline{\nabla T}$ to be an arbitrary vector, and not confined to the radial direction.

2.2 Direction Cosines of 'Line-of-Sight' in Earth Fixed Coordinate System

The GEODYN program (1976, actual version used was 7603.2) was used to generate the ephemeris of satellites in an inertial true-of-date coordinate system. The line of sight vector from GEOS-3 to ATS-6 in this coordinate system would have to be rotated by the true of date Greenwich apparent siderial time (GAST) to express it in an earth fixed coordinate system (GEODYN, 1976, Sec. 3). This was needed to determine the direction cosines of the line of sight with respect to the latitudinal, longitudinal, as well as the radial directions at GEOS-3. However, the value of GAST ($= \theta_g$) is not output by the Geodyn program with the inertial true of date output of the ephemeris of the satellites. But as the latitude, longitude and height (φ,λ,h) of the satellites is output by the program in earth fixed coordinate (E.F.C.) system, θ_g could be computed by knowing the coordinates of GEOS-3 in the two coordinate systems at the same times.

Let the E.F.C. system values of GEOS-3 be denoted by $X_\varepsilon, Y_\varepsilon, Z_\varepsilon$ and the inertial coordinate system values at the same time be denoted by X_I, Y_I, Z_I. These are related through θ_g by:

$$
\begin{aligned}
X_\varepsilon &= X_I \cos\theta_g + Y_I \sin\theta_g \\
Y_\varepsilon &= -X_I \sin\theta_g + Y_I \cos\theta_g \qquad (2.6) \\
Z_\varepsilon &= Z_I
\end{aligned}
$$

from which θ_g could be solved for. The value of $X_\varepsilon, Y_\varepsilon, Z_\varepsilon$ was available through well known formulas, e.g. (Heiskanen and Moritz, 1967, p. 182):

$$
\begin{aligned}
X_\varepsilon &= (N + h)\cos\varphi\cos\lambda \\
Y_\varepsilon &= (N + h)\cos\varphi\sin\lambda \qquad (2.7) \\
Z_\varepsilon &= [N(1 - e^2) + h]\sin\varphi
\end{aligned}
$$

where N is the radius of curvature at φ in the prime vertical direction and e^2 is the square of the first eccentricity of the ellipsoid on which φ, λ and h are defined.

After obtaining the line of sight vector in E.F.C. system, the projection of unit line of sight vector $\underline{e}_{21}$ along E.F.C. axes e_x, e_y, e_z is given by:

$$
\begin{aligned}
e_x &= (X_1 - X_2)/|\underline{R}_{21}| \\
e_y &= (Y_1 - Y_2)/|\underline{R}_{21}| \qquad (2.8) \\
e_z &= (Z_1 - Z_2)/|R_{21}|
\end{aligned}
$$

where X_1, Y_1, Z_1 and X_2, Y_2, Z_2 are now the coordinates of ATS-6 and GEOS-3 in earth fixed coordinate system, and $|\underline{R}_{21}|$ is the magnitude of the line of sight vector; and

$$\underline{e}_{21} = e_x\underline{i} + e_y\underline{j} + e_z\underline{k} \qquad (2.9)$$

where $\underline{i}, \underline{j}, \underline{k}$ are the unit vectors in the E.F.C. system.

Let the unit vectors along the geocentric spherical (r, φ', λ) coordinate system at GEOS-3 be denoted by e_r, $e_{\varphi'}$, e_λ, where the geocentric latitude φ' is obtained from:

$$\tan\varphi' = Z_2/(X_2^2 + Y_2^2)^{\frac{1}{2}} \qquad (2.10)$$

The unit vector in the (r, φ', λ) and the (X, Y, Z) in the E.F.C. system are

related through (Heiskanen and Moritz, p. 230):

$$\underline{e}_r = \cos\varphi' \cos\lambda \underline{i} + \cos\varphi' \sin\lambda \underline{j} + \sin\varphi' \underline{k}$$

$$\underline{e}_{\varphi'} = -\sin\varphi' \cos\lambda \underline{i} - \sin\varphi' \sin\lambda \underline{j} + \cos\varphi' \underline{k} \qquad (2.11)$$

$$\underline{e}_\lambda = -\sin\lambda \underline{i} + \cos\lambda \underline{j}$$

If the line of sight vector forms angles α, β, γ with the (r,φ',λ) axes, then the direction cosines a, b, c of the line of sight vector are given by the scalar product of equation (2.9) with equations (2.11), i.e.,

$$a = \cos\alpha = \underline{e}_{a_1} \cdot \underline{e}_r = e_x\cos\varphi'\cos\lambda + e_y\cos\varphi'\sin\lambda + e_z\sin\varphi'$$

$$b = \cos\beta = \underline{e}_{a_1} \cdot \underline{e}_{\varphi'} = -e_x\sin\varphi'\cos\lambda - e_y\sin\varphi'\sin\lambda + e_z\cos\varphi' \qquad (2.12)$$

$$c = \cos\gamma = \underline{e}_{a_1} \cdot \underline{e}_\lambda = -e_x\sin\lambda + e_y\cos\lambda$$

with e_x, e_y, e_z given from equation (2.8).

2.3 Covariances of Line-of-Sight Residual Acceleration

We express the gradient $\underline{\nabla T}$ of the anomalous potential in terms of its components δ_r, $\delta_{\varphi'}$, δ_λ in the (r,φ',λ) coordinates (Heiskanen and Moritz, 1967, p. 233)

$$\underline{\nabla T} = \delta_r \underline{e}_r + \delta_{\varphi'} \underline{e}_{\varphi'} + \delta_\lambda \underline{e}_\lambda \qquad (2.13)$$

$$\delta_r = \frac{\partial T}{\partial r}, \quad \delta_{\varphi'} = \frac{1}{r}\frac{\partial T}{\partial \varphi'}, \quad \delta_\lambda = \frac{1}{r\cos\varphi'}\frac{\partial T}{\partial \lambda}, \text{ or} \qquad (2.14)$$

$$\delta_r = T_r, \quad \delta_{\varphi'} = -\gamma\xi, \quad \delta_\lambda = -\gamma\eta \qquad (2.15)$$

by using equation (6.49′) of Heiskanen and Moritz (1967, p. 235), where γ is now the normal gravity at the GEOS-3 location, where the deviation of vertical components in the latitudinal and longitudinal directions are given by ξ and η.

Using equations (2.5), (2.12), (2.13), (2.15), the line of sight residual acceleration $\ddot{R}$ ($\equiv T_\ell$ for ease of notation) is given by:

$$\ddot{R} \equiv T_\ell = -\underline{\nabla T} \cdot \underline{e}_{a_1} = -aT_r + b\gamma\xi + c\gamma\eta \qquad (2.16)$$

The autocovariances of $R \equiv T_\ell$ between two points denoted by subscripts i and j are then given by 'propogation' of covariances of T_r, ξ, η by:

(2.17)

$$C_{r\ell_1,r\ell_j} \equiv (T_{\ell_1},T_{\ell_j}) = [-a_i, b_i\gamma_i, c_i\gamma_i] \begin{bmatrix} (T_{r_1},T_{r_j}), (T_{r_1},\xi_j), (T_{r_1},\eta_j) \\ (\xi_1,T_{r_j}), (\xi_1,\xi_j), (\xi_1,\eta_j) \\ (\eta_1,T_{r_j}), (\eta_1,\xi_j), (\eta_1,\eta_j) \end{bmatrix} \begin{bmatrix} -a_j \\ b_j\gamma_j \\ c_j\gamma_j \end{bmatrix}$$

$$= -a_j[-a_i(T_{r_1},T_{r_j}) + b_i\gamma_i(\xi_1,T_{r_j}) + c_i\gamma_i(\eta_1,T_{r_j})]$$

$$+ b_j\gamma_j[-a_i(T_{r_1},\xi_j) + b_i\gamma_i(\xi_1,\xi_j) + c_i\gamma_i(\eta_1,\xi_j)]$$

$$+ c_j\gamma_j[-a_i(T_{r_1},\eta_j) + b_i\gamma_i(\xi_1,\eta_j) + c_i\gamma_i(\eta_1,\eta_j)]$$

where for ease of notation, we have expressed the covariances by ( ), e.g., $C_{\xi_1,\xi_j} \equiv (\xi_1,\xi_j)$, etc.

The covariances of T_r, ξ, η were computed from subroutine COVAX (Tscherning, 1976) based on model 2 of anomaly degree variances (Tscherning and Rapp, 1974). The subroutine gives units of covariances of ξ and η in (arc seconds)^2. To convert these into units of (mgals)^2 for (T_{ℓ_1},T_{ℓ_j}), we note that expressions $(\xi_1,\xi_j),(\xi_1,\eta_j),(\eta_1,\xi_j),(\eta_1,\eta_j)$ are being multiplied by $\gamma_i\gamma_j$. As the subroutine computes the normal gravity in units of m sec^{-2}, multiplication of the covariances of ξ and η by $(10^5/\rho'')^2$ ensures units of (mgals)^2 for equation (2.17). Here ρ'' is the value of 1 radian in arc seconds. The units of the covariances of T_r were already computed in (mgals)^2 according to the modification described in Rummel et als. (1976, p. 14).

The cross-covariance between $\ddot{R} \equiv T_\ell$ at a point i and a gravity anomaly block was computed by numerical integration of the point covariance function over the mean anomaly block. A point covariance function, say at the center of anomaly block with $\ddot{R}$ at point i will be given by the following, using equation (2.16):

(2.18)
$$C_{r\ell_1,\Delta g} \equiv (T_{\ell_1},\Delta g) = -a_i(T_{r_1},\Delta g) + b_i\gamma_i(\xi_1,\Delta g) + c_i\gamma_i(\eta_1,\Delta g)$$

where the covariances have been denoted by ( ).

The computation of the autocovariance matrix of a set of $\ddot{R}$ ($\equiv T_\ell$) points used for predicting a residual mean anomaly, and the cross-covariance vector of $\underline{T}_\ell$ with the anomaly would then be done as indicated by equations (2.17) and (2.18). And, the equations (1.5) and (1.7) for the prediction, $\hat{\Delta g}'$, of residual mean anomaly, and its estimated standard deviation $\hat{\sigma}_{\Delta g'}$ would now be modified as:

(2.19)
$$\hat{\Delta g}' = \underline{C}^T_{\Delta g,r\ell}\,(\underline{\underline{C}}_{r\ell,r\ell} + \underline{\underline{D}})^{-1}\,\underline{T}_\ell = \underline{C}^T_{\Delta g,r\ell}\,\underline{\underline{C}}^{*-1}\,\underline{T}_\ell$$

(2.20)
$$\hat{\sigma}^2_{\Delta g'} = C_0 - \underline{C}^T_{\Delta g,r\ell}\,\underline{\underline{C}}^{*-1}\,\underline{C}_{\Delta g,r\ell}$$

2.4 Numerical Determination of Line-of-Sight Residual Acceleration

Before we numerically differentiate the residual range-rate $\dot{R}$ to obtain $\ddot{R}$, we need to filter the raw $\dot{R}$ values (equation (2.1)) of the observational noise. We use a cubic spline because of its well-known 'minimum norm' and 'best approximation' properties (Ahlberg, Nilson and Walsh, 1967, Chap. III) to approximate the raw $\dot{R}$ values in the least squares sense. See Sjogren et als. (1976) for similar application of cubic splines. The cubic spline is a set of cubic polynomials with adjacent polynomials meeting at the spline 'knots', where the cubic polynomials and their first and second derivatives assume the same value, making the spline a smooth twice continuously differentiable function.

Given m data points $\dot{R}_i = f(t_i)$; $i = 1, \ldots, m$ and n spline knots t_k, $k = 1, \ldots, n$; $n < m-2$ such that:

(2.21) $$t_k = t_i \quad \text{for } k = i = 1 \text{ and } k = n,\ i = m$$

we require to solve for the coefficients c^* of spline $S^* = S^*(t)$:

(2.22) $$S^*(t) = c^*_{k,3}\, d^3 + c^*_{k,2}\, d^2 + c^*_{k,1} d + S^*(t_k);$$

$$d = t - t_k,\ t_k \le t < t_{k+1},\ k = 1, \ldots, n-1, \text{ (and}$$

$S^*(t_k)$, $S^{*\prime}(t_k)$, $S^{*\prime\prime}(t_k)$ are then continuous from the right),

so that the weighted L_2 norm $\|f - S^*\|_2$ is minimized, or:

(2.23) $$\|f - S^*\|_2^2 = \sum_{k=1}^{n-1} \int_{t_k}^{t_{k+1}} w(t)\,[f(t) - S^*(t)]^2\, dt = \text{minimum},$$

and we replace the integral by summation over the data points in each of the intervals $I_k \equiv t_k \le t < t_{k+1}$

(2.24) $$\|f - S^*\|_2^2 = \sum_{i=1}^{m} w_i\, v_i^2 = \text{min., where}$$

$$v_i = v(t_i) = f(t_i) - S^*(t_i),\ i = 1, \ldots, m$$

(2.25) $$w_i = w(t_i) = (t_{i+1} - t_{i-1}) / (t_m - t_1);\ i = 2, \ldots, m-1; \text{ and}$$

$$w_1 = (t_2 - t_1) / (t_m - t_1),\ w_m = (t_m - t_{m-1}) / (t_m - t_1)$$

(i.e. for equally spaced data points, the end points are given one-half the weight of the other points (deBoor and Rice, 1968)).

The spline function in equation (2.22) gives the smoothed value of $\dot{R}$ after filtering the observational noise. The smoothing depends on the interval between the knots, giving greater smoothing as the interval between the knots is increased.

The residual acceleration $\ddot{\ddot{R}}$ is obtained by differentiating the spline function in equation (2.22):

$$\ddot{\ddot{R}} = S^{*\prime}(t) = 3c^*_{k,3}d^2 + 2c^*_{k,2}d + c^*_{k,1} \; ; \tag{2.26}$$

$$d = t - t_k \; , \; t_k \leq t < t_{k+1} \; , \; k = 1, \ldots, n-1$$

We first consider the case when the location of knots is fixed a-priori, and this is most conveniently equally spaced. The coefficients of the spline functions were solved using subroutines ICSFKU, and the smoothed values of $\dot{R}$ and $\ddot{\ddot{R}}$ by using subroutines ICSEVU and DCSEVU (IMSL, Lib. 1, Edn. 6, 1977). For details of the algorithm see deBoor and Rice (1968a). As an example, Figure 2.1 shows a plot of raw and smoothed values of $\dot{R}$ every 10 seconds for GEOS-3 revolution 439 for a-priori fixed spline knots at a nominal spacing of 100 seconds. (The actual spacing was 108 seconds with 11 spline knots for a data span of 1080 seconds.) The corresponding $\ddot{\ddot{R}}$ values are shown in Figure 2.2. For later processing, only the central values were used leaving out the first and last 4 to 5 minutes of data to avoid any spurious spline slopes at either end of data span. The initial state vectors for revolution 439 were supplied by Marsh (1978). The initial state vectors and the force model were the same as used in Marsh et als. (1977).

We next consider the case when the number of spline knots as determined above remains fixed, and we now try to obtain the optimal location for the knots by varying them one at a time to minimize the least squares error in equation (2.24). This was done using subroutine ICSVKU (IMSL, 1977). The process starts with the rightmost interior knot and proceeds sequentially to the left. The location of each knot is varied in turn to minimize the least squares error as a function of that knot. The whole process is iterated till one of several criteria of convergence is met. The criteria are chosen to achieve a desirable accuracy without doing an excessive amount of wasteful computation. (For details, see deBoor and Rice (1968b)). The location of knots at a nominal 100 seconds interval (Figures 2.1 and 2.2) is now allowed to change without changing the total number of knots. The optimal location of knots with subroutine ICSVKU and the R.M.S. value of residuals after spline fit are compared in Table 2.1 with the previous case of fixed knots.

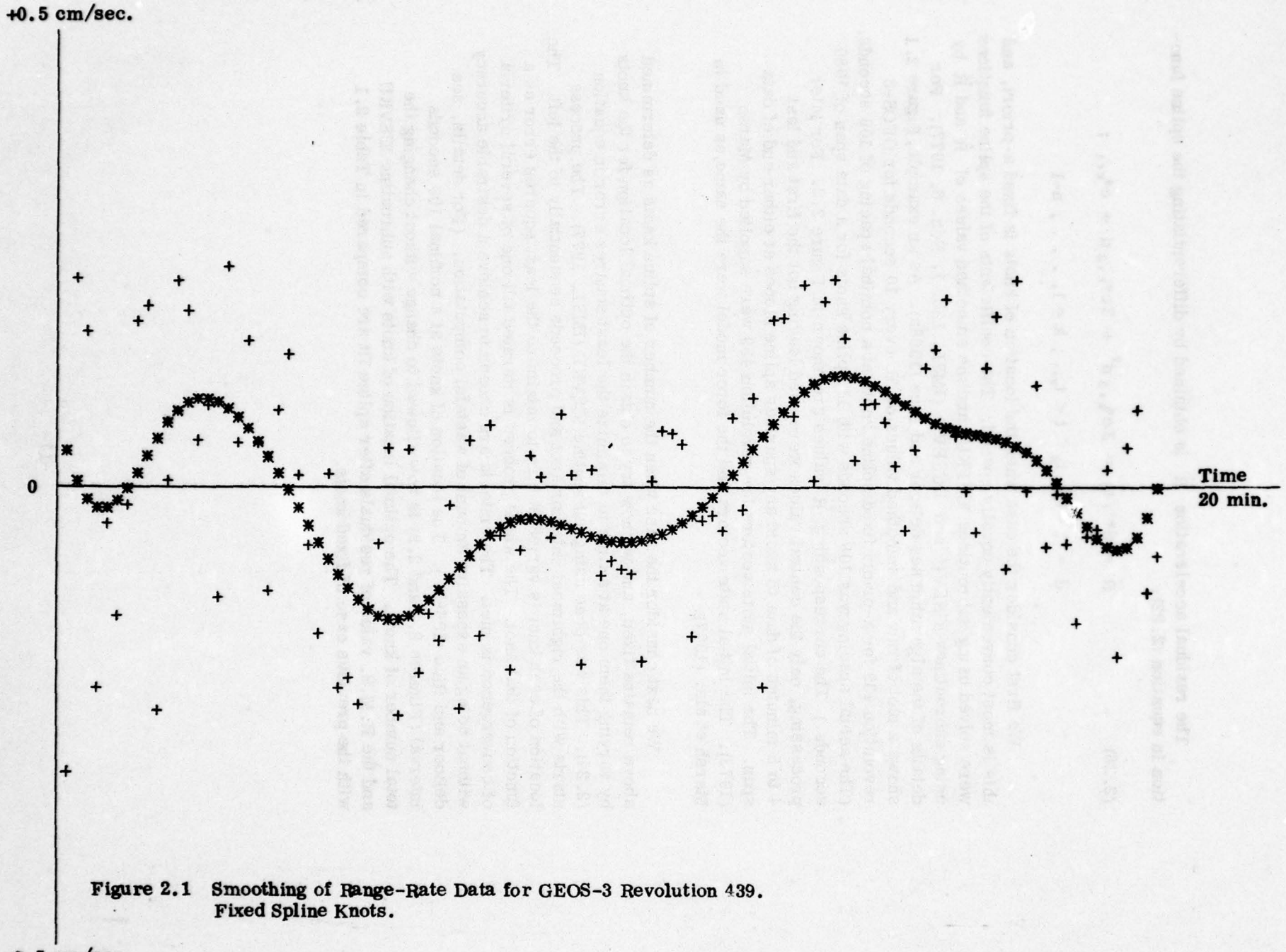

Figure 2.1 Smoothing of Range-Rate Data for GEOS-3 Revolution 439. Fixed Spline Knots.

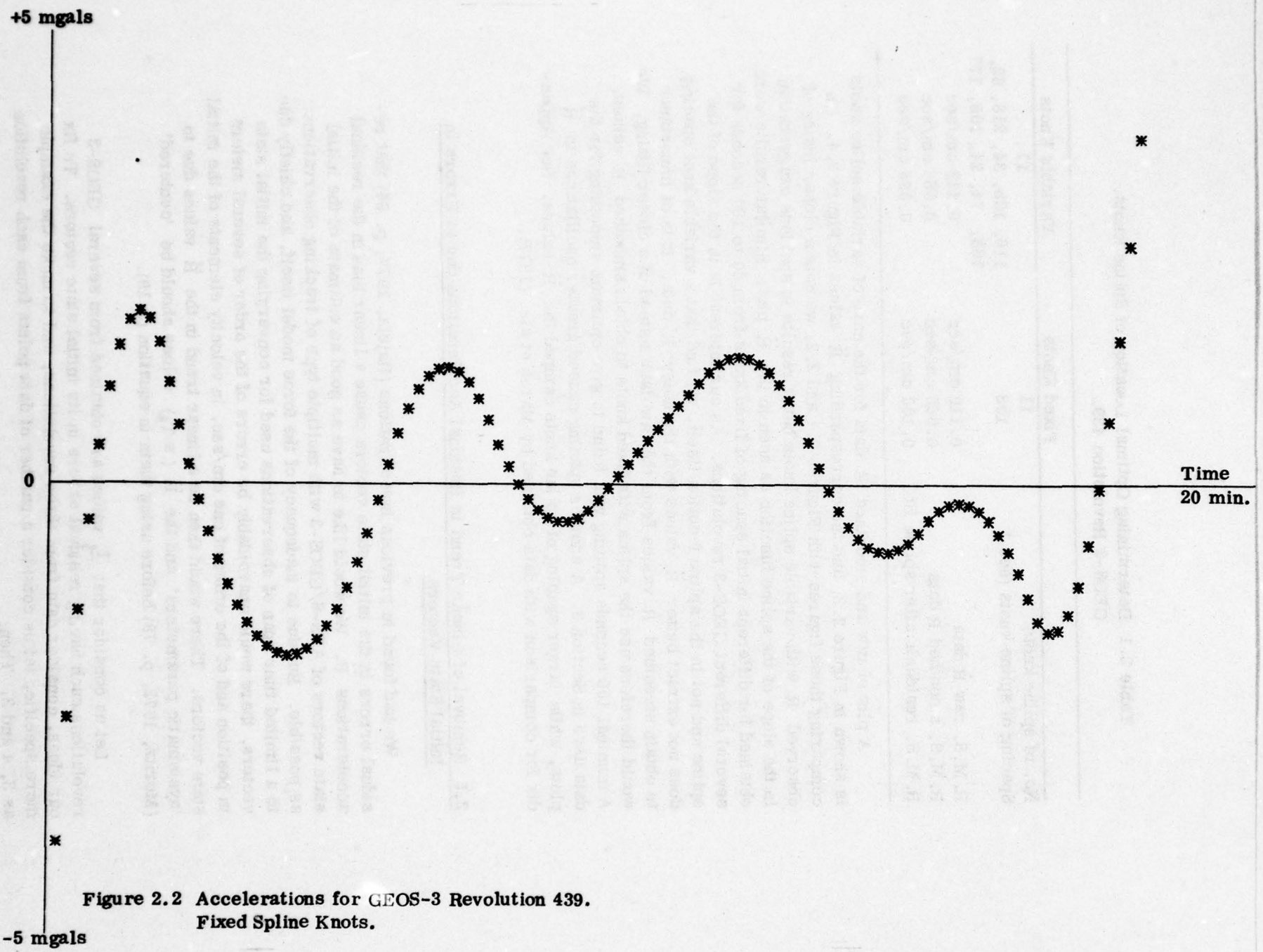

Figure 2.2 Accelerations for GEOS-3 Revolution 439.
Fixed Spline Knots.

Table 2.1 Determining Optimal Location of Spline Knots.
GEOS-3 Revolution 439.

	Fixed Knots	Variable Knots
No. of spline knots	11	11
Spacing of spline knots (sec.)	108	116, 105, 34, 218, 62, 163, 74, 24, 108, 177
R.M.S. raw $\dot{R}$ data	0.119 cm/sec	0.119 cm/sec
R.M.S. smoothed $\dot{R}$ data	0.065 cm/sec	0.068 cm/sec
R.M.S. residuals after spline fit	0.100 cm/sec	0.098 cm/sec

A plot of raw and smoothed $\dot{R}$ data for the case of variable spline knots is shown in Figure 2.3, and the corresponding $\ddot{R}$ values in Figure 2.4. On comparing these figures with Figures 2.1 and 2.2, we note a closer fitting of observed $\dot{R}$ with variable spline knots but it results in spurious exaggeration in the slope of the spline function as seen in the $\ddot{R}$ plot. Similar results were obtained for different initial spacing of fixed knots from 60 to 180 seconds for several different GEOS-3 revolutions. As our interest is in the slope of the spline and not in the spline function itself, we find that a variable knot spacing does not extract better $\ddot{R}$ values with the noisy $\dot{R}$ data. It is of importance to obtain smoothed $\dot{R}$ values from the raw data instead of a closer fitting. We would therefore use the spline with fixed knots to obtain smoothed $\dot{R}$ values. A nominal 100 seconds spacing was found to give optimum smoothing for the data used in Section 3. A shorter spacing caused greater oscillations in $\ddot{R}$ plots, while larger spacing of spline knots damped the $\ddot{R}$ values. See Appendix for comparison with data obtained by Marsh et als. (1977).

2.5 Removal of Linear Trend in Residual Accelerations due to Errors in Initial State Vectors

We had found in previous investigations (Hajela, 1977, p. 64) that residual errors in the initial state vectors cause a linear bias in the residual accelerations $\ddot{R}$. We would like to have as good an estimate of the initial state vectors of ATS-6/GEOS-3 with multiple type of tracking observations as possible. But due to inadequacy of the force model itself, and chiefly due to a limited time span of observations used for converging the initial state vectors, there would unavoidably be errors of the order of several meters in position and of the order of one cm/sec. in velocity elements of the initial state vectors. There would then be a linear trend in the $\ddot{R}$ values due to 'systematic parameters' and the $\ddot{R}$ ($\equiv T_{\ell}$) values should be 'centered' (Moritz, 1972, p. 78) before using them in equation (2.19).

Let us consider that T_{ℓ} values are obtained from several GEOS-3 revolutions each having residual errors in its initial state vectors. To fix our ideas, consider data from three revolutions, and to make the example more specific, let us consider a number of data points from each revolution as 3, 4 and 2. Then:

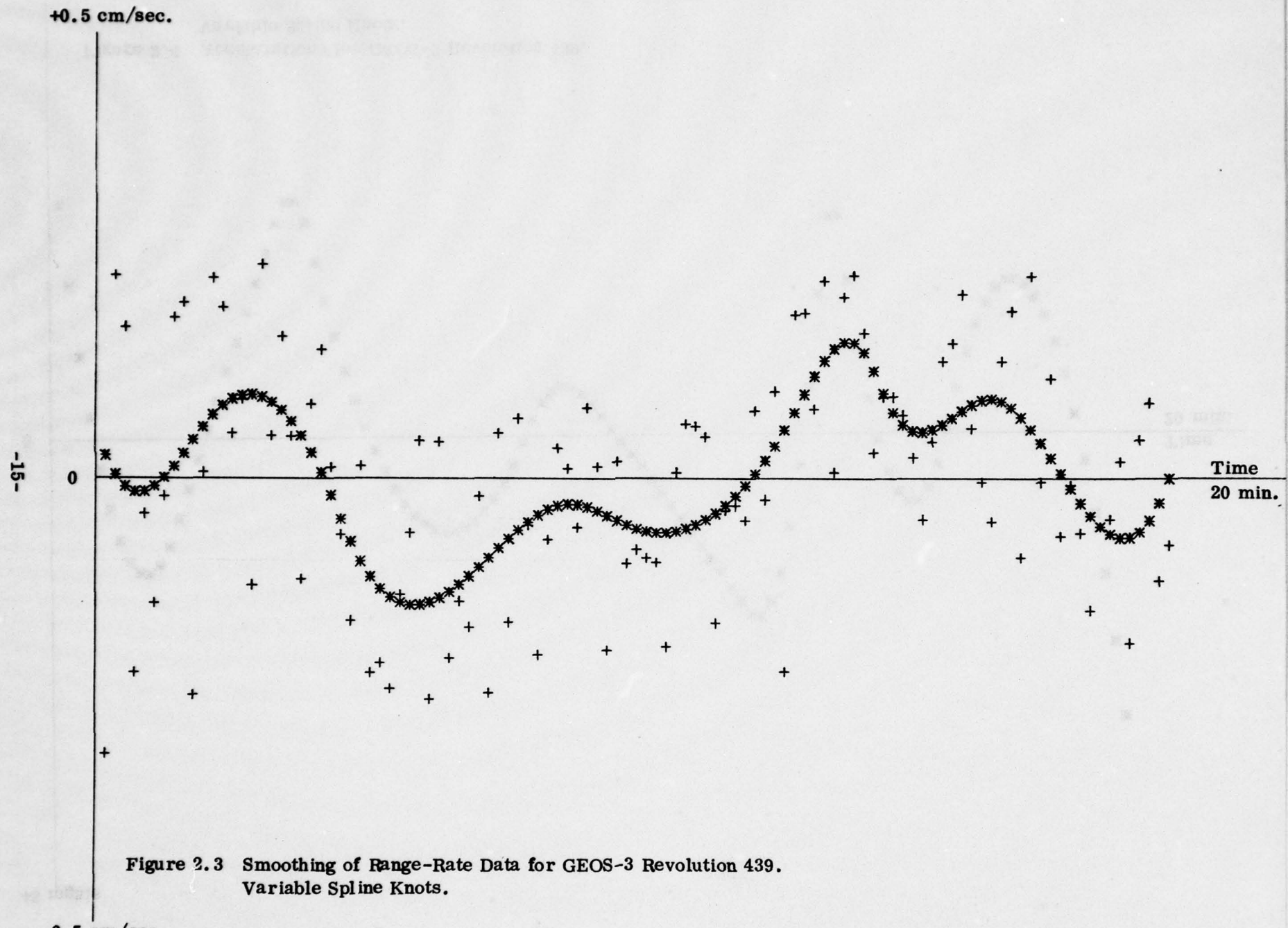

Figure 2.3 Smoothing of Range-Rate Data for GEOS-3 Revolution 439. Variable Spline Knots.

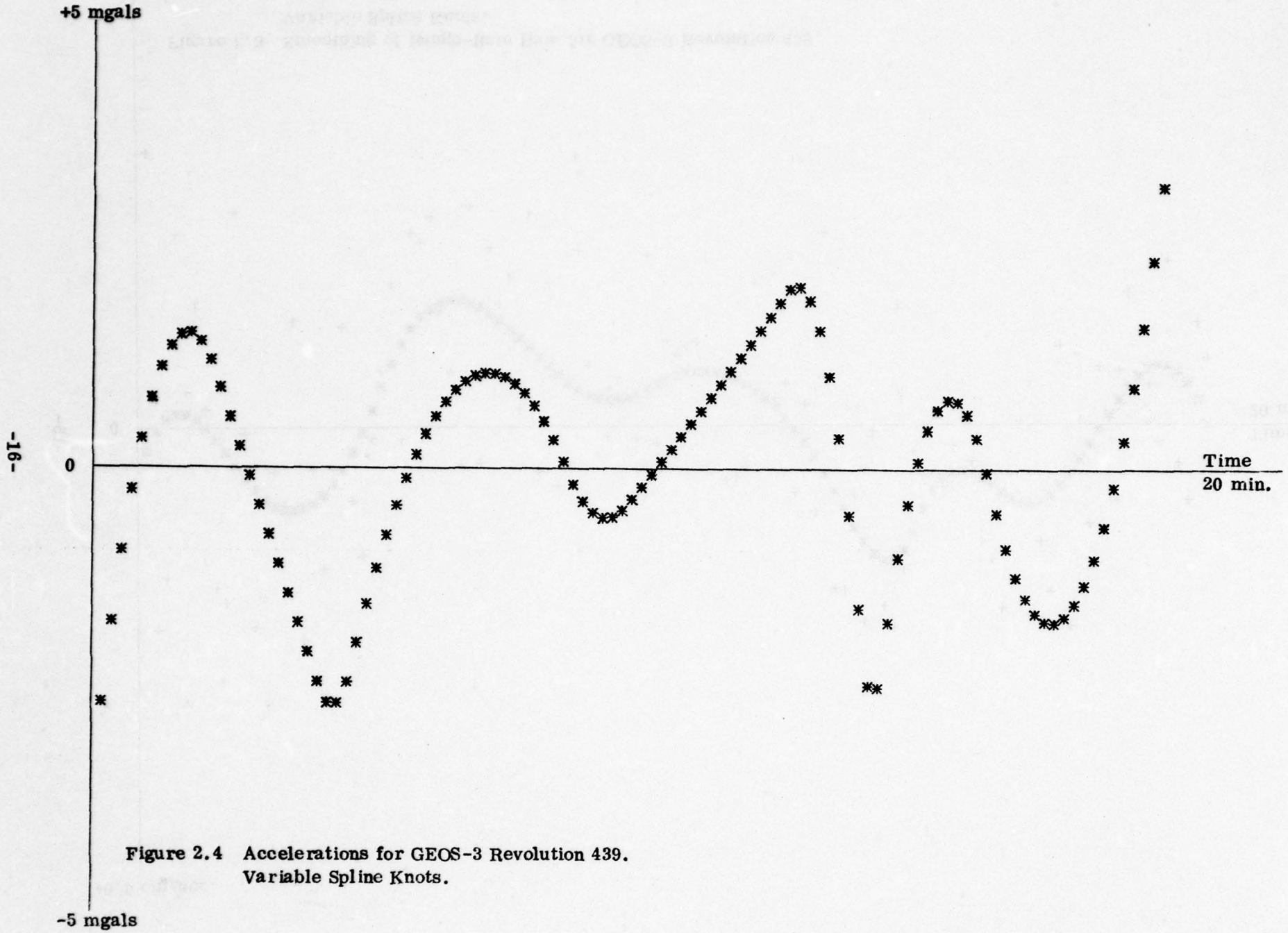

Figure 2.4 Accelerations for GEOS-3 Revolution 439.
Variable Spline Knots.

$$T_{\ell 1} = c_{11} + c_{12}(i-1) + s_i + n_i \;;\; i = 1,2,3 \quad \text{for revolution 1}$$

(2.27) $$T_{\ell 1} = c_{21} + c_{22}(i-1) + s_i + n_i \;;\; i = 1,2,3,4 \quad \text{for revolution 2}$$

$$T_{\ell 1} = c_{31} + c_{32}(i-1) + s_i + n_i \;;\; i = 1,2 \quad \text{for revolution 3}$$

where s_i and n_i are the 'signal' and the observational noise for each data point value $T_{\ell 1}$; c_{11} , c_{12} are the two parameters for the linear trend in $\underline{T}_\ell$ for data points in the first revolution. c_{11} is a zero offset and c_{12} is the slope of the linear trend. Similarly c_{21} , c_{22} for the second revolution, and so on. Using notation in Moritz (1972),

(2.28) $x^T = (T_{\ell 1}, T_{\ell 2}, \ldots, T_{\ell 9})$; $X^T = (c_{11}, c_{12}, c_{21}, c_{22}, c_{31}, c_{32})$; and

$$_9A_6 = \begin{bmatrix} 1 & 0 & & & & \\ 1 & 1 & & & & \\ 1 & 2 & & & & \\ & & 1 & 0 & & \\ & & 1 & 1 & & \\ & & 1 & 2 & & \\ & & 1 & 3 & & \\ & & & & 1 & 0 \\ & & & & 1 & 1 \end{bmatrix}$$ with the remaining elements as zero.

Equation (2.28) can be easily extended to any number of points in each revolution, say N1, N2, N3, ($N_i \geq 2$); and to any number of revolutions. Also, if instead of every T_ℓ value, say at 10 seconds interval, we use only every third value at 30 seconds interval, then the second column on the right hand side of equation (2.27), and every second column in A matrix in equation (2.28) needs to be multiplied by the interval of data points (e.g. INT = 3).

Then from equation (6.19) of Moritz (1972):

$$\underline{X} = (\underline{A}^T \underline{\underline{C}}^{*-1} \underline{A})^{-1} \underline{A}^T \underline{\underline{C}}^{*-1} \underline{x}$$

(2.29) $$\underline{\underline{C}}^* = \underline{\underline{C}}_{\tau\ell,\tau\ell} + \underline{\underline{D}}$$

$$\underline{T}^*_\ell = \underline{x} - \underline{AX}$$

and we may use the 'centered' observations $\underline{T}^*_\ell$ instead of $\underline{T}_\ell$ for predicting anomalies in equation (2.19).

The correction to $\underline{T}_\ell$ to obtain $\underline{T}^*_\ell$, i.e. the value of $\underline{AX}$ in equation (2.29) depends on the geometry of the location of data points in forming $\underline{\underline{C}}_{\tau\ell,\tau\ell}$. Also, the stability of inversion of $\underline{\underline{C}}^*$ depends on the size of the matrix, i.e. the number of data points and the assumed standard deviation of the data points in forming $\underline{\underline{D}}$. These considerations will be discussed in Section 3.3. However, a representative set of values for $\underline{AX}$ is given in Table 2.2, which was used for

predicting 5° residual anomaly number 598 with data up to a spherical distance of 3.°5 from the center of anomaly block from GEOS-3 revolutions 240, 439, 254 and 453 at 30 seconds data interval. (Details of anomalies and revolutions will be given in Section 3. The initial state vectors and the force model were the same as used in Marsh et als. (1977)). The standard deviation of data points was taken as 0.6 mgals.

Table 2.2 Removing Linear Trend from Residual Accelerations

Revolution No.	No. of Data Pts.	T_ℓ (mgals)	Correction (mgals)	T^*_ℓ (mgals)
240	1	0.0	-0.1	-0.1
	2	-0.5	0.2	-0.3
	3	-0.7	0.5	-0.2
439	1	0.4	-0.3	0.1
	2	-0.3	-0.1	-0.4
	3	-0.6	0.2	-0.4
	4	-0.6	0.5	-0.1
254	1	-0.1	0.1	0.0
	2	0.1	-0.3	-0.2
	3	0.6	-0.7	-0.1
453	1	1.0	-1.1	-0.1
	2	0.9	-1.0	-0.1
	3	0.8	-1.0	-0.2

We find that the predominant effect is to dampen the values of residual acceleration. Various combinations of data points over different anomaly blocks were tried, but invariably in all cases the value of residual accelerations was damped in trying to remove the linear trend, which would occur due to residual errors in the initial state vectors. This finally resulted in low R.M.S. values of the predicted anomalies. We have to conclude that the equation (2.29) is not sensitive enough to remove only the linear trend, and a considerable portion of the signal is also removed. The results in Section 3 would thus be reported without trying to remove the linear trend, and using equation (2.19) with $\underline{T}_\ell$, and not $\underline{T}^*_\ell$.

2.6 Correlation Between Predicted Anomalies

The variance of one predicted anomaly is given by equation (2.20). If we predict several anomalies together, the variance-covariance matrix E_{ss} of the predicted anomalies will be given by (Moritz, 1972, p. 33):

(2.30) $$\underline{\underline{E}}_{ss} = \underline{\underline{C}}_{\Delta\varepsilon,\Delta\varepsilon} - \underline{\underline{C}}_{\Delta\varepsilon,T\ell}\,(\underline{\underline{C}}_{T\ell,T\ell} + \underline{\underline{D}})^{-1}\,\underline{\underline{C}}_{T\ell,\Delta\varepsilon}$$

where $\underline{\underline{C}}_{\Delta\varepsilon,\Delta\varepsilon}$ is the variance-covariance matrix of residual anomalies of the specified block size. $\underline{\underline{C}}_{\Delta\varepsilon,T\ell}$ is the matrix with rows giving the covariance vector $\underline{C}^{T}_{\Delta\varepsilon,T\ell}$ of equation (2.20) for each anomaly with data points $\underline{T}_\ell$, and similarly the columns of matrix $\underline{\underline{C}}_{T\ell,\Delta\varepsilon}$ are the covariance vectors $\underline{C}_{\Delta\varepsilon,T\ell}$ of equation (2.20). The diagonal elements of $\underline{\underline{E}}_{ss}$ and $\underline{\underline{C}}_{\Delta\varepsilon,\Delta\varepsilon}$ are the same as $\hat{\sigma}^2_{\Delta\varepsilon'}$, and C_o in equation (2.20) for different anomalies. The correlation coefficient matrix of the predicted anomalies is obtained by dividing each row and column of $\underline{\underline{E}}_{ss}$ by the square root of the diagonal element, i.e. $\hat{\sigma}_{\Delta\varepsilon'}$. The elements of various matrices on the right hand side of equation (2.30) may by computed as discussed in Section 2.3.

However, for the purposes of numerical tests to be presented below, we used the data in Hajela (1977), i.e. covariances of $\underline{T}_r$ were used analogous to equation (1.7) instead of covariances of $\underline{T}_\ell$. In view of the very small correlations found, the tests were not repeated with $\underline{T}_\ell$ values.

We first used all the data in five GEOS-3 revolutions at a time interval of 30 seconds, a total of 83 data points in the final solution of Hajela (1977, pp. 69, 72) to predict 8 residual 5° anomalies. With a standard deviation of 1 mgal for $\underline{T}_r$ values, the largest correlation coefficient between the predicted anomalies was 0.003, and it became 0.04 when the standard deviation was taken as 1.5 mgals. The correlations are negligible as firstly, both the matrices on the right hand side of equation (2.30) are diagonal dominant, and secondly, the differencing of the matrices makes the off-diagonal terms of $\underline{\underline{E}}_{ss}$ very small.

To show this specifically, we extract the upper triangular portion of the three matrices $\underline{\underline{C}}_{\Delta\varepsilon,\Delta\varepsilon}$, $\underline{\underline{C}}_{\Delta\varepsilon,T_r}\underline{\underline{C}}^{*-1}\underline{\underline{C}}_{T_r,\Delta\varepsilon}$ and $\underline{\underline{E}}_{ss}$, for the southerly four anomalies only and show these in Table 2.3, along with the correlation coefficient matrix. The values reported are for the case of standard deviation of $\underline{T}_r$ as 1.5 mgals.

Table 2.3 Correlations Between Predicted 5° Residual Anomalies

1. $\underline{\underline{C}}_{\Delta\varepsilon,\Delta\varepsilon}$ in mgals^2	210	27	16	16
		230	-24	12
			226	33
				226
2. $\underline{\underline{C}}_{\Delta\varepsilon,T_r}\underline{\underline{C}}^{*-1}\underline{\underline{C}}_{T_r,\Delta\varepsilon}$ in mgals^2	78	31	28	23
		87	-13	23
			72	26
				61

3. $\underline{\underline{E}}_{ss}$ = (1-2) in mgals^2	132	-5	-13	-7
		143	-11	-12
			154	7
				166
4. Correlation Coefficient Matrix	1	-0.03	-0.09	-0.05
		1	-0.08	-0.08
			1	0.04
				1

We next examine if the correlation coefficients will increase if the anomaly block size being predicted is decreased to 2.°5. First $\underline{T}_r$ data from 5 GEOS-3 revolutions was used at 30 seconds interval to predict 16 2.° 5 anomalies occupying the same location as the 4 central 5° anomalies. Then the number of data points was decreased by increasing the data interval from 30 seconds to 2 minutes to 4 minutes. The largest correlation coefficient between predicted 2.° 5 residual anomalies are shown in Table 2.4. This is for 1 mgal standard deviation of $\underline{T}_r$ data. There was a slight increase in correlation coefficient when the standard deviation was increased to 1.5 mgals.

Table 2.4 Correlations Between Predicted 2.°5 Residual Anomalies

Data Intvl. Min.	No. of Data Pts.	Largest Corrln. Coeff.
0.5	66	0.10
2	15	0.28
4	5	0.30

We find that through correlation coefficients between predicted anomalies increase as the number of data points decrease, and more importantly as the anomaly block size is decreased, but the examination of correlation coefficients is not a very sensitive test because of small off-diagonal terms in $\underline{\underline{E}}_{ss}$ by differencing of two diagonal dominant matrices in equation (2.30). The larger value of the estimated standard deviation of the predicted anomaly is a better test. It was about 10 mgals for 5° anomalies and about 15 mgals for 2.° 5 anomalies. The latter value increased to about 19 mgals as the no. of data points was decreased in Table 2.4.

3. Numerical Results

We now describe some numerical tests, which are limited in nature due to the paucity of well-determined initial state vectors and thus a low incidence of data directly over the anomalies being predicted. The data was better than that used in Hajela (1977) in the sense that a better force model PGS 110 (Lerch, 1976) was used to converge the initial state vectors with adequate tracking observations (Marsh et als., 1977, p. 5). The R.M.S. value of residual range-rate $\dot{R}$, which will be reported later, was therefore smaller than used earlier (Hajela, 1977, p. 47). The available data was however still for those GEOS-3 revolutions, where the doppler signal was recorded in the 'destruct' mode. The observational noise for this type of data is expected to be about four times larger than the 'non-destruct' doppler data (Marsh et als., 1977, p. 21). Also, the data was received rather late for the present study and some discrepancies in the initial state vectors could not be reconciled in time. Data from these revolutions could therefore not be used in the present study (this will be described later in this report). However, sufficient data was analyzed to test out the improved procedures as detailed in Section 2.3.

3.1 Expected Value of Residual Anomalies

It was first intended to predict the same set of eight 5° anomalies used in Hajela (1977). But these were shifted one block westwards to better utilize the location of GEOS-3 revolutions for which the converged initial state vectors were available. The value for these anomalies, Δg_A, referred to Geodetic Reference System, 1967 (GRS 67), were available in Rapp (1977) based on altimeter data. Their terrestrial value, Δg_T, (updated in June 1978) in GRS 67 system was also available (Rapp, private communication, 1978). From these values, we subtracted the anomalies, Δg_U, implied by potential coefficients up to degree and order 12 of PGS 110 field to obtain the residual anomalies $\Delta g'_A$, $\Delta g'_T$. For comparison, we also obtained the residual anomalies, $\Delta g'_P$, implied by the potential coefficients in PGS 110 field of degree and order higher than 12. Δg_U was computed using equation (4.8) of Rummel et als. (1976, p. 20).

$$\Delta g'_A = \Delta g_A - \Delta g_U, \quad \Delta g'_T = \Delta g_T - \Delta g_U, \quad \Delta g'_P = \Delta g_P - \Delta g_U \tag{3.1}$$

The residual anomalies $\Delta g'_A$, $\Delta g'_T$, $\Delta g'_P$ are given in Table 3.1. These are the expected value $E(\Delta g')$ of the anomalies with which the predicted value $\hat{\Delta g}'$ is to be compared. The numbering of anomalies and their block sizes are according to Rapp (1977). The standard deviation of these altimeter and terrestrial anomalies was between 1 and 4 mgals.

Table 3.1 Expected Value of 5° Residual Anomalies

Seq. No.	φ_N°	φ_S°	λ_E°	λ_W°	$\Delta g'_A$ (mgals)	$\Delta g'_T$ (mgals)	$\Delta g'_P$ (mgals)
401	35	30	283	277	11.0	10.6	11.4
402	35	30	289	283	-11.0	-11.1	- 8.5
464	30	25	281	276	16.3	15.5	11.9
465	30	25	287	281	3.1	6.2	- 0.8
530	25	20	279	274	- 3.0	- 5.8	7.2
531	25	20	285	279	22.7	26.8	1.7
598	20	15	277	271	- 0.3	0.6	2.0
599	20	15	282	277	8.8	4.2	- 0.9
R.M.S. Value (mgals)					11.8	12.7	7.1

3.2 'Observed' Value of Residual Line-of-Sight Accelerations

The converged initial state vectors in the PGS 110 field for GEOS-3 revolutions used in Marsh et als. (1977, p. 26) were supplied by Marsh (private communication, 1978). Ten GEOS-3 revolutions 231, 240, 254, 268, 439, 453, 695, 709, 737 and 758, whose ground tracks were in the vicinity of the anomalies in Section 3.1, were chosen for the present study. The destruct mode doppler data (NASA, 1975) for these revolutions was preprocessed (Martin, 1975) to give range-rate sum ($\dot{R}_S$) observations. These $\dot{R}_S$ values were then used in the GEODYN program (1976, actual version used was 7603.2) in the data reduction mode in the reference gravitational field U described by potential coefficients up to degree and order 12 in the PGS 110 field. The initial state vectors of ATS-6/GEOS-3 were constrained to the values supplied by assigning them very low variances. This gave us the inertial true of date ephemeris of the satellites and their latitude, longitude and height, and the residual range-rate $\dot{R}$ as in equation (2.1).

The $\dot{R}$ values were compared with those quoted in Marsh et als. (1977, Appendix) and agreed within ± 0.01 cm/sec and less for 6 revolutions 240, 254, 439, 453, 737 and 758. The slight variation was perhaps due to differences in applying ionospheric corrections during pre-processing. However, the $\dot{R}$ values differed by about .02 cm/sec for revolution 231, about .03 cm/sec for revolution 695, about .3 cm/sec for revolution 268 and about .5 cm/sec for revolution 709. The discrepancy in the last four revolutions was most likely due to some wrong numbers in the initial state vectors used, but this could not be reconciled in time for this study. Thus the $\dot{R}$ values in only the first six revolutions was processed further.

About 20 minutes of raw $\dot{R}$ data in each revolution was approximated in the least squares sense by a cubic spline with fixed knots at a nominal spacing of 100 seconds, as described in Section 2.4. The time span for fitting the spline was longer by about 4 to 5 minutes at each end, as the smoothed $\dot{R}$ values were needed for only the central 10 minutes. This was to avoid any spurious exagger-

ation in the spline slope ($\ddot{R}$) at the ends of data span. The R.M.S. value of raw $\dot{R}$, smoothed $\dot{R}$, and the 'observational' noise filtered by the spline (R.M.S. residuals after spline fit) are given in Table 3.2.

Table 3.2 Smoothing of 'Observed' Residual Range-Rate $\dot{R}$ by Cubic Spline

Revolution No.	R.M.S. Value in cm/sec.		
	Raw $\dot{R}$	Smoothed $\dot{R}$	Residuals after Spline Fit
240	.116	.069	.092
254	.086	.061	.061
439	.119	.065	.100
453	.104	.074	.074
737	.110	.047	.100
758	.129	.103	.078

We note that the 'observational noise' is large as compared to the smoothed $\dot{R}$, and the signal noise ratio of 2:1 assumed in Marsh et als. (1977, p. 15) is too optimistic for at least the revolutions in Table 3.2. The large noise is not due to over-smoothing by the cubic spline function, but perhaps a result of recording the doppler signal in the destruct mode. Several other splines with fixed knots at 60, 80, 100 seconds etc. were tried with the present data, but the R.M.S. value of residuals after spline fit did not change by more than 4 to 6%. On the other hand, a closer fitting of raw $\dot{R}$ data led to spurious oscillations in $\dot{R}$, i.e. the slope of the spline.

The $\ddot{R}$ values were obtained from the spline function representing smoothed $\dot{R}$ values as in equation (2.26), and this is the 'observed' residual line of sight acceleration in Sections 2.1 to 2.3. These $\ddot{R}$ ($\equiv \underline{T}_\ell$) values in each revolution were then separately used to predict by equations (2.19) and (2.20) those residual anomalies, whose centers were within a spherical distance of 7.°5 from the data in the revolution. This showed by a rough comparison if the doppler data in any revolution had any system bias, and hence poor $\ddot{R}$ data, which would lead to a poor recovery. Because of the iterative nature of converging the initial state vectors, there is a possibility of system bias not becoming apparent, if the time span for the fitted observations is only over one revolution. The comparison is rough because we cannot expect a good recovery from only one revolution. But it does highlight poor data by comparing the R.M.S. value of the predicted anomalies $\hat{\Delta g'}$ (equation (2.19)) with the R.M.S. value of the expected anomalies $E(\Delta g')$ (equation (1.6)), and by examining the R.M.S. value of anomaly discrepancies $\epsilon(\Delta g')$:

$$\epsilon(\Delta g') = \hat{\Delta g'} - E(\Delta g') \tag{3.2}$$

These are shown in Table 3.3 for each of the six revolutions.

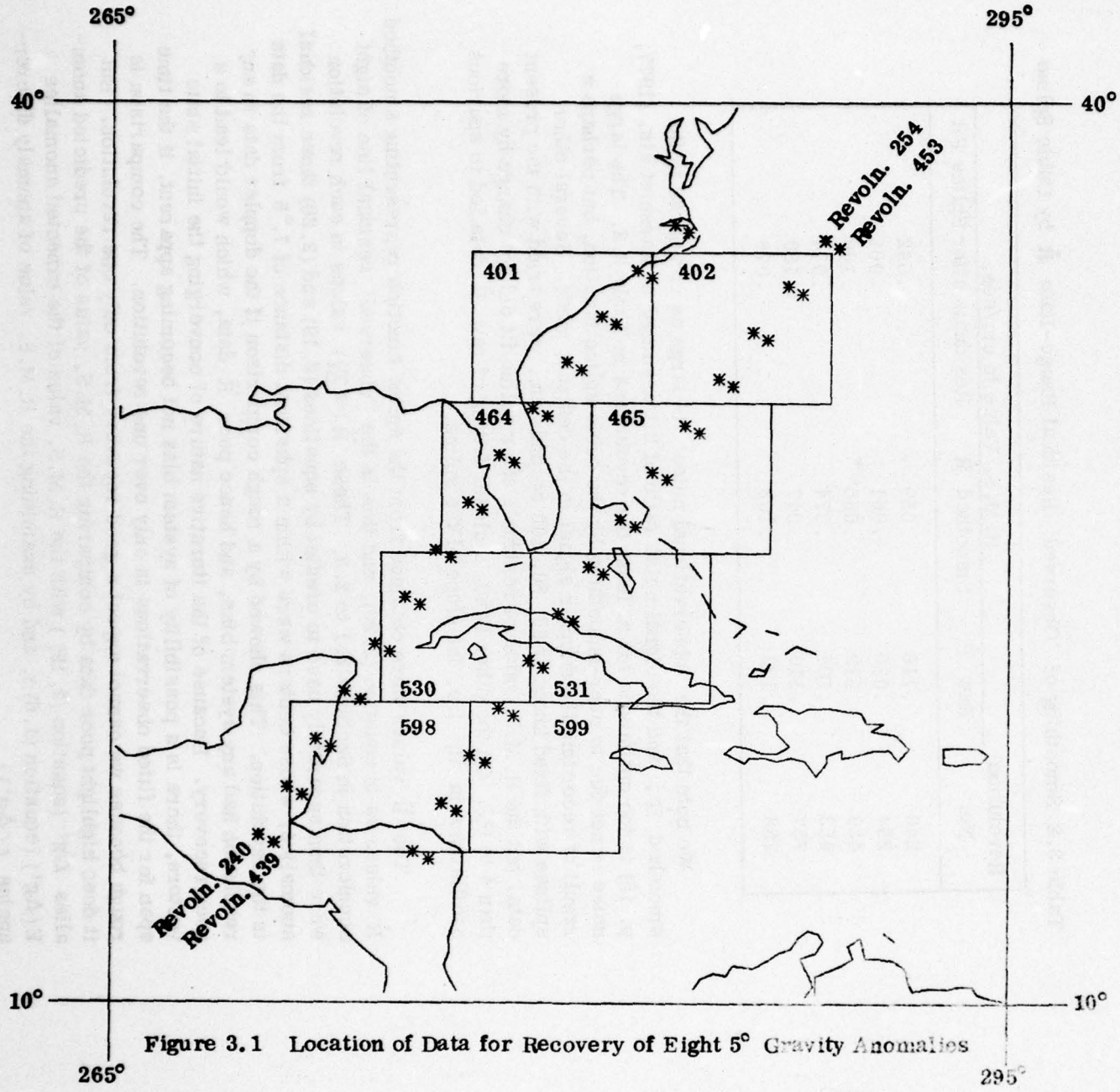

Figure 3.1 Location of Data for Recovery of Eight 5° Gravity Anomalies

Table 3.3 Examining Residual Accelerations Separately in Each GEOS-3 Revolution by Predicting Anomalies

Revolution No.	R.M.S. Value in mgals			No. of Anom.
	Expected Value	Predicted Value	Anom. Discrepancy	
240	12	5	11	8
254	12	5	9	8
439	12	5	10	8
453	12	6	9	8
737	13	2	13	4
758	13	4	13	6

Because of comparatively lower R.M.S. value of predicted anomalies and higher R.M.S. value of anomaly discrepancies, we decided to omit the $\ddot{R}$ data in revolutions 737 and 758 from the final solution. The subsatellite points for GEOS-3 revolutions 240, 254, 439 and 453 are shown in Figure 3.1 at 30 seconds interval with respect to the eight 5° anomalies being predicted. This is rather sparse data, particularly as it senses the anomalies from almost the same locations in revolutions 240 and 439, and revolutions 254 and 453, the ground tracks of these revolutions being quite close. We will first describe a few other numerical considerations, and present the final solution in Section 3.4. A comparison of raw and smoothed $\dot{R}$ data, and $\ddot{R}$, used in this study with values quoted in Marsh et als. (1977) is given in the appendix. The values of $\ddot{R}$ agreed within ±0.5 mgals.

3.3 Numerical Considerations in the Prediction of Anomalies

It was found that the most critical test for the recovery of anomalies was a low R.M.S. value of the anomaly discrepancies coupled with a closer agreement of the R.M.S. value of the predicted anomalies to that for the expected values (Table 3.1). Several tests were therefore carried out to examine the effect on these two considerations of the size of area in which several anomalies may be predicted simultaneously as in Section 2.6. Other tests were conducted to examine the effect of different assumed standard deviation of $\ddot{R}$ ($\equiv T_\ell$) data, and the time interval of $\ddot{R}$ data. Also the number of subdivisions of 5° mean anomalies to numerically integrate the point covariances to obtain the covariance for the mean anomaly. This was required in the computation of $\underline{C}_{\Delta\varepsilon, \tau\ell}$ in equations (2.19) and (2.20) by a single numerical integration over the mean anomaly, and in the computation C_o in equation (2.20) by a double numerical integration over the mean anomaly. A summary of these findings is presented below.

Firstly, it was found that the larger the area over which data was considered for the $\underline{\underline{C}}^*$ matrix, the poorer the anomaly recovery was. This was found whenever several anomalies were predicted at a time from a larger block of $\underline{T}_\ell$

data. It was therefore necessary to predict each anomaly separately considering the data for a given spherical distance from the center of that anomaly block. The same effect was also found when the extent of data was reduced for predicting one 5° anomaly block by considering data up to a spherical distance of 3.°5 from the center of the block instead of 5° or 7.°5. This is obviously related to the numerical stability of the inversion of $\underline{\underline{C}}^*$ matrix comprising of the point covariances of T_ℓ at GEOS-3 altitudes. The smaller the extent of data the more numerically stable the inversion of $\underline{\underline{C}}^*$.

The stability of inversion of $\underline{\underline{C}}^*$ was very strongly dependent on the assumed standard deviation of $\underline{T}_\ell$. We recall from equations (2.19) and (2.20) that $\underline{\underline{D}}$ was a diagonal matrix with each element being the variance of $\underline{T}_\ell$, making $\underline{\underline{C}}^*$ a diagonal dominant matrix with increase in assumed standard deviation. For standard deviation lower than 0.5 mgals, $\underline{\underline{C}}^{*-1}$ was numerically unstable, but with standard deviation higher than 1.5 mgals, $\underline{\underline{C}}^{*-1}$ was damped. This directly effected the sensitivity of $\underline{\underline{C}}_{\Delta\varepsilon,\tau_\ell}\,\underline{\underline{C}}^{*-1}$ with which $\underline{T}_\ell$ data is multiplied in equation (2.19) to obtain the predicted value of the anomaly. The optimum standard deviation of $\underline{T}_\ell$ was dependent on the extent of $\underline{T}_\ell$ data. Several standard deviations were tried between 0 and 1.2 mgals in steps of 0.2 mgals. It appeared that a standard deviation of 0.6 mgals was optimum for data up to 3.°5 from the center of 5° anomaly block, while 1 mgal may be suitable for data up to 7.°5 from the center of anomaly block.

The optimum interval of $\underline{T}_\ell$ data was found to be 30 seconds with a linear separation of about 1.°5. The R.M.S. value of anomaly discrepancies was about the same whether the time interval of data was 30 seconds or 1 minute, but there was a slight favorable increase in the R.M.S. value of predicted anomalies with data interval of 30 seconds. Any further reduction in time interval would be wasteful of computer time without proportionate benefit.

The estimated standard deviation $\hat{\sigma}_{\Delta\varepsilon'}$ in equation (2.20) was not very sensitive to the above tests. It would show slight decrease with the reduction in extent of data, and slight decrease with the decrease in data interval to 30 seconds instead of 1 minute. It would also increase with increase in standard deviation of $\underline{T}_\ell$ data. However, $\hat{\sigma}_{\Delta\varepsilon'}$ was quite sensitive to the multiple 'sensing' of the anomaly. It showed definite improvement as data from more revolutions was used over an anomaly block.

For the numerical integration of point covariances to compute covariance for the mean anomaly, the 5° block was first subdivided into 25 portions. That is, the mean anomaly covariance was obtained as the mean of point covariance computed at the center of each component 1° block. Later the 5° block was subdivided into 100 portions, which utilized the mean of 4 point covariances in each component 1° block. There was only a slight difference in the covariance vector $\underline{\underline{C}}_{\Delta\varepsilon,\tau_\ell}$ and the related quantities, i.e. $\underline{\underline{C}}_{\Delta\varepsilon,\tau\ell}\,\underline{\underline{C}}^{*-1}$ and the predicted anomaly $\hat{\Delta g}'$ in equation (2.19), or in the second term on the right hand side of equation (2.20). But there was a marked reduction in C_o, and therefore in the estimated

standard deviation $\hat{\sigma}_{\Delta s}$, of the predicted anomaly by about 2 to 3 mgals. Of course, there was also a more than twice the increase in computer time. An efficient strategy would therefore be to subdivide the 5° mean anomaly block into 25 portions for the computation of $\underline{C}_{\Delta s, \tau_\ell}$, and into 100 portions for the computation of C_o. Later, for production runs C_o may be computed once and kept in a table for being read in for slightly different sized 5° equal area blocks instead of being computed again and again. A similar approach was used by Rapp (1977).

3.4 Recovery of 5° Residual Anomalies

Based on the numerical tests described in Section 3.3, the prediction of each residual anomaly (and we now call them simply as anomalies) was done one at a time considering $\underline{T}_\ell$ data up to a spherical distance of 3.°5 from the center of the 5° block. All data from four GEOS-3 revolutions 240, 254, 439 and 453 shown in Figure 3.1 which fell inside the 3.°5 spherical distance was used to predict eight anomalies individually. The time interval of data was 30 seconds with an assumed standard deviation of 0.6 mgals. The point covariances were computed as detailed in Section 2.3 and covariances involving the mean anomaly were computed by numerical integration after subdividing the 5° anomaly into 25 subdivisions. The estimated standard deviation of the predicted anomaly was however computed with the variance C_o of the mean anomalies of the given block size being computed with 100 subdivisions. As discussed in Section 2.4, smoothed value of the residual range-rate $\dot{R}$ was obtained by fitting the raw $\dot{R}$ data in the least squares sense by a cubic spline function with fixed spline knots at a spacing of 100 seconds. The $\ddot{R}$ ($\equiv T_\ell$) data obtained by analytical differentiation of the spline function was not filtered any further for removal of any linear trend due to errors in initial state vectors.

The predicted residual anomalies were examined against their expected values (Table 3.1) for three cases, i.e. against values which were determined by altimeter data, or terrestrial data, or by the potential coefficients in the PGS 110 field. The predicted anomalies are listed in Table 3.4 along with the expected values based on altimeter data, and the anomaly discrepancies. The estimated standard deviation of the predicted anomaly is also given.

Table 3.4 Comparison of Predicted Anomalies with Altimeter Anomalies

Seq. No.	φ_N°	φ_S°	λ_E°	λ_W°	Residual Anom. (mgals) Expected	Predicted	Discrepancy	Std. Devn. (mgals)
401	35	30	283	277	11	4	-7	7
402	35	30	289	283	-11	-8	3	6
464	30	25	281	276	16	11	-5	7
465	30	25	287	281	3	4	1	5
530	25	20	279	274	-3	6	9	6
531	25	20	285	279	23	11	-12	5
598	20	15	277	271	0	-6	-6	4
599	20	15	282	277	9	5	-4	7
R.M.S. Value in mgals					12	7	7	(Mean) 6

Summary statistics of the comparison of the predicted anomalies with each of the three expected values are given in Table 3.5. This consists of the R.M.S. values of the expected anomalies, predicted anomalies and the maximum, minimum, mean and R.M.S. value of the anomaly discrepancies. For comparison between the three cases, correlation coefficient, ρ, between the predicted and expected anomalies is also given.

$$(3.3) \qquad \rho = \left(\sum_{i=1}^{n} \hat{\Delta g'}_i \, E(\Delta g'_i)/n\right) \Big/ \left(\left(\sum_{i=1}^{n} \hat{\Delta g'}_i{}^2/n\right)^{\frac{1}{2}} \left(\sum_{i=1}^{n} E(\Delta g'_i)^2/n\right)^{\frac{1}{2}}\right)$$

The standard deviation of the predicted anomalies is already given in Table 3.4.

Table 3.5 Summary Comparison of Predicted Anomalies with Altimeter, Terrestrial and PGS 110 Anomalies

Comparison with Anomalies from	R.M.S. Expected Value (mgals)	R.M.S. Predicted Value (mgals)	Anomaly Discrepancy (mgals) Max.	Min.	Mean	R.M.S.	Corr. Coeff. ρ
Altimeter data	12	7	9	-12	-3	7	0.85
Terrestrial data	13	7	12	-16	-3	8	0.79
P.G.S.110 field	7	7	8	- 8	0	5	0.71

For comparison of predicted anomalies with altimeter anomalies, the R.M.S. value of the predicted anomalies is lower (7 mgals instead of expected 12 mgals), because of few GEOS-3 revolutions directly over the predicted anomalies. The lack of revolutions also shows up as mean anomaly discrepancy being -3 mgals, primarily because of predicted anomaly 531 being only 11 instead of 23 mgals (Table 3.4). However, inspite of insufficient density of observations, the effectiveness of the prediction procedures is borne out by R.M.S. anomaly

discrepancy (7 mgals) being comparable to the mean of estimated standard deviation of predicted 5° anomalies (6 mgals), and the high correlation coefficient, 0.85, of predicted and expected anomalies.

The predicted anomalies agree better with altimeter anomalies than with terrestrial anomalies. At first sight, it might appear that the predicted anomalies agree most closely (except for lower correlation coefficient ρ) with PGS 110 anomalies. This is so because the PGS 110 field was complete only up to degree and order 30, and therefore inadequate to recover the 5° anomalies (note the low R.M.S. value of 7 mgals for the residual 5° anomalies implied by PGS 110). Because of insufficient data, the R.M.S. value of the predicted anomalies is also low, and therefore the predicted and PGS 110 anomalies appear to agree more closely.

It is of great interest to determine if the predicted anomalies in this report are an improvement over the anomalies implied by PGS 110 field. This is shown in Table 3.6 with statistics similar to Table 3.5. However, we now show the comparison of both the predicted anomalies and PGS 110 anomalies with the anomalies determined from altimeter data.

Table 3.6 Improvement of Predicted Anomalies over Anomalies Implied by PGS 110 Field. Comparison with Altimeter Anomalies.

Comparison with Altimeter Anomalies of	R.M.S. Value (mgals)		Anomaly Discrepancy (mgals)				Corr. Coeff.
	Altimeter Anomalies	Predicted/ PGS 110 Anom.	Max.	Min.	Mean	R.M.S.	ρ
Predicted Anomalies	12	7	9	-12	-3	7	0.85
PGS 110 Anomalies	12	7	10	-21	-3	9	0.62

We note that inspite of insufficient density of observations (Figure 3.1), the predicted anomalies agree much better with the altimeter anomalies, as compared to the agreement of PGS 110 anomalies with the altimeter anomalies. It is expected that the agreement of predicted anomalies with altimeter anomalies would be significantly improved if there was greater density of observation.

4. Summary and Conclusions

The doppler signal count in SST provides a direct measure of the range-rate sum ($\dot{R}_s^o$) from GEOS-3 to ATS-6 to the ground station in the earth's gravitational field. The range-rate ($\dot{R}$) from GEOS-3 to ATS-6 in the anomalous field T is obtained by subtracting from $\dot{R}_s^o$ a computed value of range-rate sum ($\dot{R}_s^c$) based on the computed orbits of the two satellites in the normal reference gravitational field, U. U was taken complete to degree and order 12 in PGS 110 field (Lerch, 1976) and the force model (including solar radiation pressure, luni-

solar gravitation, atmospheric drag, etc.) completely described the motion of ATS-6. The raw $\dot{R}$ values had 'observational' noise due to doppler count being in the 'destruct' mode in the revolutions used for this study, besides any residual errors in the 'converged' initial state vectors used for integrating the orbits of the two satellites.

The raw $\dot{R}$ values were filtered of the 'noise' and smoothed by fitting them with a cubic spline function with fixed knots. The R.M.S. value of residuals after the spline fit (i.e. R.M.S. value of the noise) for 4 revolutions used in this study varied from 0.06 to 0.10 cm/sec., and was equal to or larger than the smoothed $\dot{R}$ values which had R.M.S. value from 0.06 to 0.07 cm/sec. (Table 3.2). The prediction of anomalies from $\ddot{R}$ (time-derivative of smoothed $\dot{R}$) was therefore severely limited by the data noise. It is expected that, in future, the 'non-destruct' doppler data would have a noise-level of about one-fourth that of 'destruct' doppler data (Marsh et als., 1977, p. 21). The prediction is also limited because of paucity of present data (Figure 3.1) as it consisted of just about one revolution directly over the anomaly block being predicted. This resulted in a low R.M.S. value of the predicted anomalies. An optimum data density (Hajela, 1977) would have been about two times that used in this study.

The initial state vectors for the 4 revolutions were the same as used in Marsh et als. (1977), and details about the data used for their 'convergence' is given in Table 1 (ibid., p. 26). Two approaches were tried to extract a 'better' signal (of $\ddot{R}$) from the raw $\dot{R}$ values. One was to 'center' the observations (Moritz, 1972, p. 78) for any systematic linear 'trend' in raw $\dot{R}$ values due to residual errors in the 'converged' initial state vectors. The second was to fit the raw $\dot{R}$ values with a spline function with variable knots (deBoor and Rice, 1968b). Both these approaches led to negative results. Firstly, any attempt to remove a linear trend led to severe damping of 'observed' $\dot{R}$ values and thus a loss of signal. We have to therefore accept an independent 'determination' of the 'converged' values of initial state vectors based on long (several revolutions, preferably over several days) time-span of different types of observations (Hajela, 1977). Secondly, the spline function with fixed knots was preferable to approximate the raw $\dot{R}$ values, as the variable knots led to large and sudden changes in the spline slope, i.e. in $\ddot{R}$. There was greater need to choose the 'smoothing' over 'fitting' of raw $\dot{R}$ values out of the conflicting requirements of these two processes in obtaining $\ddot{R}$ values.

The residual acceleration $\ddot{R}$ in the anomalous field T represents the projection of its gradient vector, ∇T, at GEOS-3 in the 'line of sight' GEOS-3 to ATS-6 in the 'hi-lo' SST (equation (2.5)). The auto-covariances of the three components of ∇T in the radial, latitudinal and longitudinal directions and their cross-covariances with gravity anomalies were obtained from subroutine COVAX (Tscherning, 1976). The direction cosines of the line of sight were determined from the computed satellite orbits. The auto and cross-covariances of $\ddot{R}$ could then be computed rigorously, and this is a major contribution of this study. The prediction of anomalies using these covariances, and the $\ddot{R}$ values, follows from equations (2.19) and (2.20).

The numerical considerations in the prediction of anomalies have been outlined in Section 3.3. The actual computational strategy based on these considerations has been summarized in the beginning of Section 3.4. An important finding is that these procedures lead to the computation of covariances with each anomaly separately and therefore to the prediction of anomaly by collocation independently of the prediction of neighboring anomalies. The correlation coefficients between the predicted values of neighboring anomalies is almost zero (Section 2.6).

We realize that because of the paucity of data, and also due to the 'high' noise-level of destruct doppler data, we cannot draw strong conclusions from the numerical results in Section 3.4. Nevertheless, Tables 3.4 and 3.5 clearly demonstrate the effectiveness of the procedures developed in this study. 5° anomalies can be recovered from the ATS-6/GEOS-3 SST doppler data with a standard deviation of about 6 mgals. This is likely to improve further with greater density of data, and with the use of 'non-destruct' doppler data. It is most interesting that inspite of the limitations of the data used in this study, the predicted 5° anomalies are an improvement (Table 3.6) over the anomalies implied by the (30,28) PGS 110 field.

References

Ahlberg, J.H., E.N. Nilson and J.L. Walsh, The Theory of Splines and Their Applications, Academic Press, New York, 1967.

DeBoor, C. and J.R. Rice, Cubic Spline Approximation I-Fixed Knots, II-Variable Knots, Computer Sciences Department TR 20, 21, Purdue University, April, 1968.

Eddy, W. and R. Sutermeister, Satellite to Satellite Measurements, Wolf Research and Development Group, Riverdale, Maryland, August, 1975.

GEODYN System Description, Vol. I, Parts 1 and 2, Wolf Research and Development Group, Riverdale, Maryland, August, 1976.

GRS 67 (Geodetic Reference System, 1967), Publ. Spéc. du Bull. Géod., Central Bureau of the International Association of Geodesy, Paris, 1971.

Hajela, D.P., Direct Recovery of Mean Gravity Anomalies from Satellite to Satellite Tracking, Department of Geodetic Science Report No. 218, The Ohio State University, Columbus, December, 1974.

Hajela, D.P., Recovery of 5° Mean Gravity Anomalies in Local Areas from ATS-6/GEOS-3 Satellite to Satellite Range-Rate Observations, Department of Geodetic Science Report No. 259, The Ohio State University, Columbus, September, 1977.

Heiskanen, W. and H. Moritz, Physical Geodesy, W.H. Freeman and Co. San Francisco, 1967.

IMSL (International Mathematical and Statistical Libraries, Inc.), Library 1, Edition 6, Houston, 1977.

Kaula, W.M. (Editor), The Terrestrial Environment: Solid Earth and Ocean Physics, Report of a Study at Williamstown, Massachusetts, August, 1969.

Lerch, F.J., The PGS-110 Gravity Model, Private Communication, Goddard Space Flight Center, Greenbelt, Maryland, 1976.

Marsh, J.G., B.D. Marsh, T.D. Conrad, W.T. Wells and R.G. Williamson, Gravity Anomalies near the East Pacific Rise with Wavelengths Shorter than 3300 km Recovered from GEOS-3/ATS-6 Satellite to Satellite Doppler Tracking Data, NASA T.M. 79553, Goddard Space Flight Center, Greenbelt, Maryland, December, 1977.

Marsh, J.G., Private Communication (Initial State Vectors for ATS-6/GEOS-3), Goddard Space Flight Center, Greenbelt, Maryland, August, 1978.

Martin, C.F., Geodyn Modifications for Satellite to Satellite Tracking and Surface Density Layer Estimation, Wolf Research and Development Corporation, Riverdale, Maryland, February, 1972.

Martin, T.V., Private Communication (ATS-R Preprocessor Program), Wolf Research and Development Group, Riverdale, Maryland, September, 1975.

Moritz, H., Advanced Least Squares Methods, Department of Geodetic Science Report No. 175, The Ohio State University, Columbus, June, 1972.

NASA, Geos-C Mission Plan, Wallops Island, Virginia, May, 1974.

NASA, ATS-6/GEOS-3 SSE Tracking Data Supplement for 4/9/75 - 6/28/75, April, 1976.

Rapp, R.H., Mean Gravity Anomalies and Sea Surface Heights Derived from GEOS-3 Altimeter Data, Department of Geodetic Science Report No. 268, The Ohio State University, Columbus, December, 1977.

Rapp, R.H., Private Communication (5° Mean Terrestrial Gravity Anomalies, 1978 update), The Ohio State University, Columbus, July, 1978.

Rummel, R., L.P. Hajela and R.H. Rapp, Recovery of Mean Gravity Anomalies from Satellite-Satellite Range Rate Data Using Least Squares Collocation, Department of Geodetic Science Report No. 248, The Ohio State University, Columbus, September, 1976.

Rummel, R. and R.H. Rapp, Covariances of Line of Sight Residual Accelerations, Unpublished Notes, The Ohio State University, Columbus, August, 1977.

Rummel, R., Ch. Reigber and K.H. Ilk, The Use of Satellite to Satellite Tracking for Gravity Parameter Recovery, European Workshop on Space Techniques for Solid Earth, Oceanography, Navigation and Geodesy, Schloss Elmau, 1978.

Sjogren, W.L., P.A. Laing, A.S. Liu and R.N. Wimberley, GEOS-3 Experiment Final Report: Analysis of SST Doppler Data for the Determination of Earth Gravity Field Variations, Jet Propulsion Laboratory, May, 1976.

Tscherning, C.C. and R.H. Rapp, Closed Covariance Expressions for Gravity Anomalies, Geoid Undulations, and Deflections of the Vertical, Implied by Anomaly Degree Variance Models, Department of Geodetic Science Report No. 208, The Ohio State University, Columbus, May, 1974.

Tscherning, C.C., Covariance Expressions for Second and Lower Order Derivatives of the Anomalous Potential, Department of Geodetic Science Report No. 225, The Ohio State University, Columbus, January, 1976.

Appendix

Comparison of residual range-rate $\dot{R}$ (raw and smoothed data) and residual accelerations $\ddot{R}$ obtained in this study with those in Marsh et als. (1977).

The force field and the initial state vecotrs used in this study were provided by Marsh (1978), and are the same as in Marsh et als. (ibid.). The differences in the raw $\dot{R}$ in this study and in Marsh et als. is perhaps due to the difference in applying ionospheric corrections during preprocessing. The smoothed $\dot{R}$ and $\ddot{R}$ values were obtained by different procedures in the two studies. In both studies, the data was generated every 10 seconds. This has been extracted at 1 minute interval in the following tables.

REVOLUTION 240

Observation Time			GEOS-3 Subsatellite Point		Present Study			Marsh et als. (1977)		
					$\dot{R}$ in cm/sec.		$\ddot{R}$	$\dot{R}$ in cm/sec.		$\ddot{R}$
YYMMDD	HHMM	SEC	LAT.	E. LONG	Raw	Smoothed	mgals	Raw	Smoothed	mgals
750426	2306	24.	38.4	285.9	-0.068	-0.101	-0.0	-0.074	-0.096	-0.1
750426	2307	24.	35.4	283.4	-0.235	-0.090	0.4	-0.242	-0.097	0.1
750426	2308	24.	32.4	280.9	-0.031	-0.059	0.7	-0.039	-0.066	0.7
750426	2309	24.	29.3	278.7	0.059	-0.009	0.9	0.050	-0.015	0.7
750426	2310	24.	26.2	276.5	0.039	0.053	1.1	0.029	0.042	1.0
750426	2311	24.	23.0	274.5	0.052	0.115	0.9	0.042	0.103	0.7
750426	2312	24.	19.8	272.5	0.200	0.149	0.1	0.189	0.125	-0.1
750426	2313	24.	16.7	270.6	0.132	0.116	-1.0	0.121	0.098	-0.6
750426	2314	24.	13.4	268.7	0.093	0.054	-0.9	0.081	0.050	-0.7

REVOLUTION 254

Observation Time			GEOS-3 Subsatellite Point		Present Study			Marsh et als. (1977)		
					$\dot{R}$ in cm/sec.		$\ddot{R}$	$\dot{R}$ in cm/sec.		$\ddot{R}$
YYMMDD	HHMM	SEC	LAT.	E. LONG	Raw	Smoothed	mgals	Raw	Smoothed	mgals
750427	2251	24	38.4	291.4	-0.032	0.046	0.2	-0.038	0.033	0.1
750427	2252	24.	35.4	288.8	0.186	0.036	-0.6	0.180	0.021	-0.5
750427	2253	24.	32.4	286.4	0.009	-0.016	-1.0	0.002	-0.021	-0.7
750427	2254	24.	29.3	284.1	0.034	-0.058	-0.2	0.027	-0.053	-0.3
750427	2255	24.	26.1	282.0	-0.137	-0.046	0.5	-0.145	-0.051	0.3
750427	2256	24.	23.0	279.9	0.031	-0.005	0.8	0.022	-0.013	0.7
750427	2257	24.	19.8	277.9	0.100	0.036	0.5	0.092	0.023	0.4
750427	2258	24.	16.6	276.0	0.080	0.054	0.1	0.072	0.042	0.2
750427	2259	24.	13.4	274.2	0.191	0.064	0.4	0.182	0.065	0.4

REVOLUTION 439

Observation Time			GEOS-3 Subsatellite Point		Present Study			Marsh et als. (1977)		
					$\dot{R}$ in cm/sec.		$\ddot{R}$	$\dot{R}$ in cm/sec.		$\ddot{R}$
YYMMDD	HHMM	SEC	LAT.	E. LONG	Raw	Smoothed	mgals	Raw	Smoothed	mgals
750511	0041	54.	37.7	285.9	0.060	-0.047	0.8	0.061	-0.061	0.6
750511	0042	54.	34.7	283.4	-0.050	-0.034	-0.3	-0.049	-0.040	0.0
750511	0043	54.	31.6	281.0	-0.072	-0.053	-0.2	-0.072	-0.045	-0.1
750511	0044	54.	28.5	278.8	0.052	-0.041	0.6	0.053	-0.032	0.4
750511	0045	54.	25.4	276.7	0.068	0.012	1.2	0.069	0.017	1.0
750511	0046	54.	22.2	274.6	0.070	0.084	1.0	0.071	0.078	0.7
750511	0047	54.	19.1	272.7	0.026	0.108	-0.3	0.027	0.094	-0.2
750511	0048	54.	15.9	270.8	0.037	0.074	-0.6	0.038	0.077	-0.2
750511	0049	54.	12.7	268.9	-0.044	0.052	-0.2	-0.043	0.058	-0.4

REVOLUTION 453

Observation Time			GEOS-3 Subsatellite Point		Present Study			Marsh et als. (1977)		
					$\dot{R}$ in cm/sec.		$\ddot{R}$	$\dot{R}$ in cm/sec.		$\ddot{R}$
YYMMDD	HHMM	SEC	LAT.	E. LONG	Raw	Smoothed	mgals	Raw	Smoothed	mgals
750512	0026	34.	38.7	292.3	0.041	-0.046	-0.5	0.037	-0.038	-0.5
750512	0027	34.	35.7	289.7	-0.055	-0.059	0.0	-0.057	-0.059	-0.1
750512	0028	34.	32.6	287.3	-0.062	-0.056	0.0	-0.064	-0.060	0.0
750512	0029	34.	29.5	285.0	-0.084	-0.069	-0.6	-0.086	-0.078	-0.5
750512	0030	34.	26.4	282.8	-0.132	-0.105	-0.4	-0.133	-0.100	0.0
750512	0031	34.	23.2	280.8	-0.055	-0.088	1.0	-0.055	-0.070	0.8
750512	0032	34.	20.1	278.8	0.083	-0.004	1.5	0.083	-0.007	1.0
750512	0033	34.	16.9	276.9	0.188	0.069	0.8	0.188	0.058	0.9
750512	0034	34.	13.7	275.0	0.162	0.103	0.3	0.162	0.102	0.4